The influence of pipeline wettability and crude oil composition on deposition of gas hydrates during petroleum production

Guro Aspenes

Thesis for the degree of Philosophiae Doctor (PhD)
at the University of Bergen

2009

Guro Aspenes

Department of Chemistry

University of Bergen

Allégaten 41

N-5007 Bergen

Norway

Preface

This thesis, submitted for the degree of Philosophiae Doctor at the University of Bergen, consists of seven papers and a summary of the work. The work has been performed at the Department of Chemistry, University of Bergen in the period 2006-2009. From January 2009 until July 2009 I had a stay at the Hydrate Research Center at Colorado School of Mines, in Golden, Colorado, USA. The work has been financed by the Norwegian Research Council and the industry partners Statoil R&D (originally Hydro R&D) and Chevron in the HYADES project, a KMB-project. The HYADES (HYdrate Agglomeration and DEpostion Studies) project is interdisciplinary, combining physical chemistry, petroleum chemistry, physics and the industrial aspects in research on hydrate plugging.

Prevention of hydrate plugs in petroleum production pipelines is important for the petroleum industry, and today large amounts of methanol or glycol are used to prevent plugs from forming. The work presented in this thesis consists of determining the influence of pipeline material and crude oil composition on the deposition of hydrates to the pipeline wall during petroleum transportation. Reduction of hydrates depositing onto the pipeline wall will probably reduce the plugging tendency, which can have positive economical and environmental effects.

Acknowledgements

I would like to thank my supervisors Sylvi Høiland, Tanja Barth and Kjell Magne Askvik. A special thank to my main supervisor, friend and colleague Sylvi for her support and inspiration. You have always been there for me, helping me, encouraging me, and made me believe in myself and in my work. Even in tight schedules you have found time for me. Tanja Barth should also be thanked for her open door and being exceptionally knowledgeable in organic and petroleum chemistry. I would also like to thank the Norwegian Research Council, Statoil R&D (originally Hydro R&D) and Chevron for financing my Ph.D. thesis. ARTA AS should be thanked for supplying the metal samples, free of charge, which was used throughout this study.

The HYADES project group should be thanked for pushing me further with recommendations on the way forward. Maren A. Dahl (Master student in Physics at UoB) should be thanked for enhancing the understanding of influence of flow on adhesion of water/hydrates to the pipeline wall.

Thanks to my friends and colleagues who made the Department of Chemistry a good working environment, Anna, Shiva, Djurdjica, Kristin, Espen, James, Ina and Andreas. I would also like to thank the rest of the staff at the Department.

Thanks to SINTEF Petroleum Research and the people at the Bergen office for inviting me into their working space giving me an office in their premises, making me feel included. A special thank to Boris Balakin for being my office mate and making the office an efficient working environment. Sylvi, Anna, Djurdjica and Roar should be thanked for always being open

Abstract

At specific temperature and pressure conditions, hydrates can sometimes plug production pipelines. It has been shown that some oils contain natural inhibiting compounds (NICs) that prevent hydrate plug formation even though the pressure and temperature are within the hydrate formation conditions. Thus, the hydrate plugging tendency is influenced by the crude oil composition. The mechanisms by which deposition of hydrates occur in a petroleum production system are also likely to be related to pipeline surface properties, e.g. pipeline material, surface free energy and roughness.

The ultimate aim of this work is to develop an understanding of the deposition of hydrates on the pipeline wall. Most of the work in this thesis deals with contact angle measurements that determine the wettability of various solids. Different materials and oil compositions have been tested including both model oil systems and crude oil systems. Micromechanical force experiments have been used to determine the adhesion force between hydrates and solids with different amounts of petroleum acids present in the oil phase.

The factors that have been identified in this work as most likely influencing deposition of hydrates to the pipeline wall are the presence of free water, surface material and crude oil composition. It may seem as if hydrate deposition will not occur unless free water is present. When the pipeline wall material has a low surface free energy, such as epoxy coated surfaces, deposition seems to be reduced. Crude oils that are assumed as non-plugging and contain high concentrations of acids seems to reduce the probability for deposition to occur.

List of Publications

Papers

- Paper I: Hydrate Agglomeration and Deposition Studies - HYADES, S. Høiland, A.E. Borgund, G. Aspenes and P. Fotland, Proceedings of Oil Field Chemistry Symposium (OFCS), March 08, Geilo, Norway.

- Paper II: The influence of petroleum acids and solid surface energy on pipeline wettability in relation to hydrate deposition, G. Aspenes, S. Høiland, T. Barth, K.M. Askvik, Journal of Colloid and Interface Science 333 (2009) 533-539.

- Paper III: Wetting properties of rough epoxy coated pipeline surfaces in relation to gas hydrate deposition, G. Aspenes, S. Høiland, T. Barth, Submitted in November 09.

- Paper IV: Wettability of petroleum pipelines: influence of crude oil and pipeline material in relation to hydrate deposition, G. Aspenes, S. Høiland, A.E. Borgund, T. Barth, Energy & Fuels 24 (2010) 483-491.

- Paper V: Hydrate Agglomeration and Deposition Studies - the influence of pipeline wettability and flow, G. Aspenes, B. Balakin, A.E. Borgund, S. Høiland, Proceedings of Oil Field Chemistry Symposium (OFCS), March 09, Geilo, Norway.

- Paper VI: Adhesion force between cyclopentane hydrates and solid surface materials, G. Aspenes, L.E. Dieker, Z. Aman, S. Høiland, A.K. Sum, C.A. Koh, E.D. Sloan, Accepted for publication in Journal of Colloid & Interface Science (DOI: 10.1016/j.jcis.2009.11.071).

- Paper VII: Influence of model oil with surfactants and amphilic polymers on cyclopentane hydrate adhesion forces, Z.M. Aman, L.E. Dieker, G. Aspenes, A.K. Sum, E.D. Sloan, C.A. Koh, Accepted for publication in Journal of Colloid & Interface Science, January 2010.

Abbreviations

ADSA-D	Axisymmetric Drop Shape Analysis - Diameter
ADSA-P	Axisymmetric Drop Shape Analysis - Profile
CyC5	Cyclopentane
DDDC	Dual-Drop Dual Crystal
DLVO	Derjaguin-Landau-Vervey-Overbeek
EDL	Electrical Double Layer
EOS	Equation of state for interfacial tension
EtO	Ethylene oxide
IEP	Isoelectric point
LDHI	Low Dosage Hydrate Inhibitor
MEG	Monoethylene glycol
MeOH	Methanol
MMF	Micromechanical Adhesion Force
NIC	Natural hydrate Inhibiting Components
NIR	Near Infrared
PCA	Principal Component Analysis
ppm	Parts per million
PZC	Point of Zero Charge
SEM	Scanning Electron Microscopy
TAN	Total Acid Number
TBAB	Tetra-n-butyl ammonium bromine
TBN	Total Base Number
THF	Tetrahydrofuran

Symbols

θ	Contact angle
θ_{exp}	Experimental obtained contact angle
θ_e	Young's contact angle
θ_a	Advancing angle
θ_r	Receding angle
$\Delta\theta$	Contact angle hysteresis, θ_a-θ_r
θ_w	Wenzel contact angle
γ_{ab}	Interfacial tension between a and b
γ_c	Surface tension of c
W_{abc}	Adhesion energy between a and b in c
β	Constant for EOS
R_a	Average roughness
R_t	Maximum height
r_{si}	Surface index
r_w	Wenzel's roughness factor
A_n	Ratio between roughness and change in contact angle
V	Droplet volume
r	Needle radius
F	Correction factor
g	Acceleration due to gravity
ρ	Density
P_{cap}	Capillary pressure
r_n, $n = 1$ or 2	Principal radii of curvature of solid surface
F_{cap}	Capillary force
D	Height of liquid meniscus

d	Height of wetting on particle
R^*	Harmonic mean radius
R_n, $n = 1$ or 2	Radius of a sphere or solid surface
F_{adh}	Adhesion force
δ	Separation distance
k	Capillary spring constant
Re	Reynolds number
N	Pipeline velocity
D_{pipe}	Pipeline diameter
μ	Viscosity
a	Particle diameter
$|v_y^{(0)}|$	Initial particle velocity

Contents

Chapter 1

Introduction

Pipeline plugging during petroleum production and transport is a major problem for the petroleum industry. Hydrate plugging in sub-sea pipelines is the most significant problem in flow assurance [1]. Natural gas hydrates are similar to ice and are formed at low temperatures and high pressures. Prevention of hydrate formation by heating, insulation or the use of inhibitors is very expensive. On the Norwegian Continental Shelf, the most common strategy to completely preventing hydrate formation is to use large amounts of alcohols and glycols. There has been a paradigm change in thinking over the last few years, moving from total prevention of hydrates to risk management [2]. This implies that, as long as hydrates flow with the stream and do not agglomerate or deposit onto the pipe walls, the plugging tendency will be reduced.

This work deals with hydrate deposition onto the pipeline wall, where the effect of pipeline material and crude oil composition is studied. Pipelines used for petroleum transportation are affected over time by the fluids and solids with which they are in contact, giving rise to corrosion, coating by an oil or wax/asphaltene layer, or general wear. The deposition of hydrates in

a production line is likely to be affected by the state of the pipe wall. The pipeline walls are the coldest point in the system, providing an excellent nucleation and growth site if hydrate formation conditions are met [3]. Nicholas et al. [4] recently confirmed that hydrates will deposit onto the pipeline wall by using a condensate flow loop. However, micromechanical force measurements indicate that free water has to be present for deposition to occur [4]. Capillary bridging is necessary for hydrates to aggregate and lead to pipeline plugging [5,6].

Crude oils vary in their potential for forming hydrate plugs, indicating that some oils contain natural compounds that act as anti-agglomerants [7]. Anti-agglomerants are surface-active and are able to adsorb to the hydrate surface, and presumably also the pipeline surface, creating oil-wet conditions. This reduces the possibility of hydrogen-bonding between hydrate particles, and between a hydrate particle and the pipeline wall, reducing agglomeration and deposition, respectively. Several authors [8–12] have suggested that the inhibiting components are contained in the acid fraction of the crude oil, however little is known about the specific structures of active compounds in the acid fraction.

Chapter 2

Gas Hydrates

Natural gas hydrates are crystalline inclusion compounds composed of water and gas, resembling ice in structure and appearance. The gas molecules (guests) are trapped inside water cages (host) that are composed of a hydrogen-bonded network of water molecules [13], as illustrated in Figure 2.1.
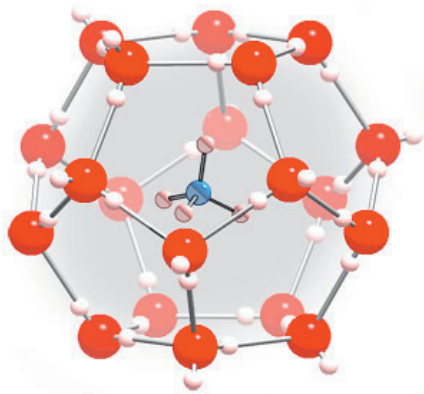

Figure 2.1: Simplified illustration of a cage created from hydrogen bonded water molecules with an enclathrated methane guest molecule, which is a part of a petroleum pipeline hydrate structure. The figure is taken from the homepage of University of California [14].

3

Hydrate research can be divided into three historical periods [13]:

- From the discovery of gas hydrates in 1810 where the progress has been driven by the scientific curiosity of water and gas transforming into a solid.

- The identification of hydrates plugging pipelines in the petroleum industry, starting from 1934.

- Hydrates were discovered in nature both in deep oceans and in permafrost in the 1960s. Hydrates in the earth have been considered as being both an energy resource (due to the large amount of methane gas stored) and an environmental hazard which could lead to global warming upon dissociation.

Recent research focuses on gas hydrates as a means for energy storage, transportation and for separating gas and water, which are novel techniques that are under development. Indeed, in one volume unit of gas hydrates, up to 164 standard volumes of methane gas can be stored.

This work deals with the formation of gas hydrate plugs during petroleum production. The first hydrate plug was identified by Hammerscmidt in 1934 [15]. It was first believed that the plug was ice, however when the plug had a higher melting point than ice, it was verified as a hydrate plug.

2.1 Hydrate structures

Hydrates can exist as several different structures, depending on the guest molecules (gas). The three most common hydrate structures are described in Figure 2.2. The gas component most frequently present in crude oil is

methane; ethane and propane are also present in small quantities. Non-flammable, non-hydrocarbon components, like carbon dioxide and nitrogen, are often present in trace amounts and are regarded as contaminants [16]. Methane and ethane are small molecules, and these gases form Structure I hydrates when present individually. When methane and ethane are present simultaneously, as in petroleum pipelines, structure II will be formed [13]. Propane is a larger molecule and Structure II hydrates are needed to provide cavities of suitable size [13]. Structure H normally contains two or more types of guests.
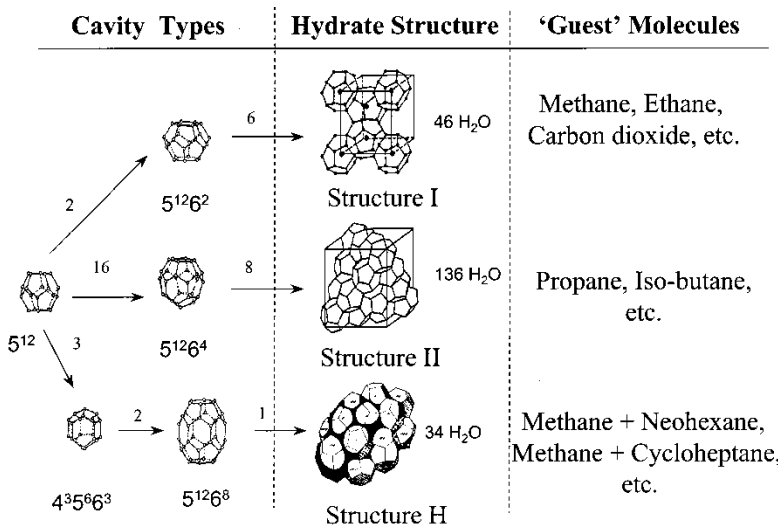

Figure 2.2: The three most common hydrate unit crystal structures. Nomenclature: $5^{12}6^4$ indicates a water cage composed of 12 pentagonal and 4 hexagonal faces. Numbers of cage types are indicated along the lines. Example: the Structure I unit crystal is composed of 2 5^{12} cages, 6 $5^{12}6^2$ cages, and 46 water molecules. The figure is from Sloan [17].

2.2 Formation of hydrates

Hydrates can be formed when the pressure and temperature region for hydrate formation is reached, as shown in the phase diagram in Figure 2.3. Hydrates can be formed in the region to the left of the line. Temperatures are typically $< 27\ °C$ and pressures are typically > 6 bar [17]. Different gases give different phase diagrams. Within the pressure and temperature conditions for hydrate formation, some period of time is often required for hydrates to form and this is normally termed the induction time [1]. The hydrate crystals can grow into large clusters of hydrates.
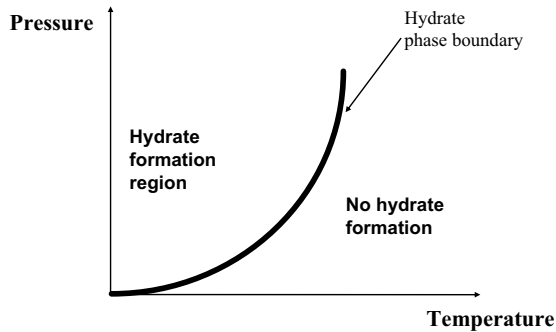
Figure 2.3: Simplified illustration of a hydrate phase diagram. Hydrates are formed at high pressures and low temperatures.

2.3 Industrial aspects: Inhibition of hydrates

Hydrate plug formation is one of the largest problems in flow assurance [13]. When hydrate plugs are formed, they constitute a danger due to the pressure build-up, and are very expensive due to delay in production. The most common strategy to prevent hydrate formation in the petroleum industry is to operate outside the thermodynamic conditions of hydrate formation. This

can be achieved by designing production facilities so that normal day-to-day production conditions are located outside hydrate formation region, e.g. by avoiding long sub-sea pipes which would lead to low temperatures.

In areas where hydrate formation is unavoidable, the strategy used by most operators in Norway involves addition of a thermodynamic inhibitor, typically methanol (MeOH) or monoethylene glycol (MEG), in order to inhibit hydrate formation [13]. MeOH is very popular due to its low cost and effectiveness. Nevertheless, the use of methanol has become so expensive that methanol recovery and return lines are becoming more common. Glycols are less volatile compared to alcohols and are thereby easier to regenerate. However, one mass percent of MeOH inhibits hydrate formation more than an equivalent mass percent of glycol in aqueous liquid. For gas dominated systems, MEG is frequently preferred to MeOH due to recovery. The choice of MeOH versus MEG may be determined by economic considerations. In many North Sea applications, glycols are the preferred inhibitor.

When adding MeOH or MEG to the water phase in production pipelines, the hydrate phase diagram can be changed. Lower temperatures and higher pressures are required for hydrate formation to occur, as illustrated in Figure 2.4, where the phase boundary, with addition of inhibitors (solid line), is compared to the original phase boundary (dashed line). The phase boundary moves as a function of amount of added inhibitor up to a limit of approximately 30 % for MeOH. Hemmingsen et al. [5] have actually shown that under-inhibition (low insufficient amount of inhibitor) may increase the plugging tendency and deposition of hydrates to the pipeline wall, compared to uninhibited systems (no inhibitor present).

Other alternatives for avoiding hydrates are insulation, which will only work for a given length, and heating, which could work for any pipeline
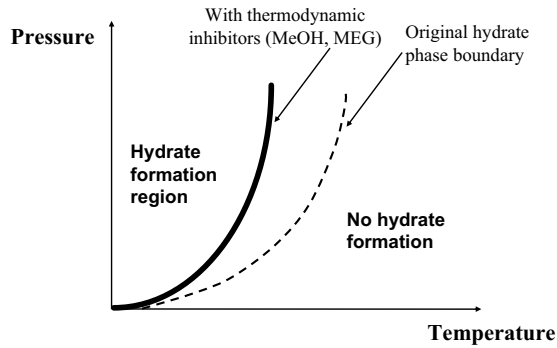
Figure 2.4: Simplified illustration of a hydrate phase diagram. Addition of thermodynamic inhibitors such as methanol and monoethylene glycol lead to a change in the hydrate phase boundary (solid line) moved to the left (lower temperatures) from the original phase boundary (dashed line).

length. However, both heating and insulation are expensive and, in many cases, are not considered realistic. Yet another alternative is the use of low dosage hydrate inhibitors (LDHI), which inhibit hydrate formation when added in low concentrations, i.e. 0.1-1.0 wt% [18]. However, there is a major limitation with LDHIs, due to their low efficiency at low temperatures (sub-cooling of 20 °F) [13].

Some crude oils have shown to be unproblematic with regard to plugging, even when operated within thermodynamic conditions for stable hydrate formation. Several authors have indicated that the plugging tendency of crude oils is dependent on the presence or absence of natural inhibiting components (NICs) [7,8,19,20]. A possible mechanism could be the adsorption of special surface active compound types to the hydrate surface, preventing the small hydrate particles from agglomerating into large plugs.

2.4 Models for gas hydrates

In this thesis, the experimental work has not involved natural gas hydrates, due to extreme temperature and pressure conditions associated with natural gas hydrates. Instead, this work uses models for natural gas hydrates, denoted as hydrate formers, which are easier and safer to work with in the laboratory. The choice of hydrate former for use in experiments is based on criteria such as miscibility with water, hydrate structure, hydrate formation temperature, toxicity and volatility. Ice contamination may influence experiments performed with hydrate formers that are miscible with water and that has relatively low hydrate formation temperatures. Some hydrate formers usually used in laboratory experiments as models for the natural gas hydrates, are mentioned below.

2.4.1 Cyclopentane hydrates

Cyclopentane (CyC5), C_5H_{10}, forms Structure II hydrates below 7.7 °C at 1 atm [13]. Similar to pipeline hydrate formers, CyC5 is immiscible in water. CyC5 hydrates are used in adhesion force experiments with the micromechanical force apparatus, described in Section 5.3.2.

2.4.2 TBAB hydrates

Tetra-n-butyl ammonium bromine (TBAB) forms hydrates of both structure I and II depending on the concentration of TBAB and the temperature. An aqueous solution of > 20 wt% TBAB only form structure I hydrates, with hydrate formation below 10 °C at 1 atm [21]. An aqueous solution of < 20 wt% TBAB may form either structure I or structure II hydrates dependent on the temperature [21]. TBAB is only soluble in the water phase since it

is a salt. TBAB is used as a hydrate former in the detachment experiments; see Section 6.4.

2.4.3 Tetrahydrofuran hydrates

Tetrahydrofuran (THF) forms structure II hydrates below 4.4 °C at 1 atm [13]. THF is a cyclic ether and is completely miscible in water. THF is highly volatile and may evaporate easily.

2.4.4 Ethylene oxide hydrates

Ethylene oxide (EtO) forms structure I hydrates below 11.1 °C at 1 atm [13]. EtO is a cyclic ether and is completely miscible in water. EtO is also highly volatile and may evaporate easily.

2.4.5 Freon hydrates

Trichlorodifluoromethane (R-11), CCl_3F, or Freon (R-11) forms structure II hydrates below 8.5 °C at 1 atm [13]. Freon has previously been used as a refrigerant, but is being replaced because of ozone depletion effects.

Chapter 3

Pipeline surface properties

Pipeline surface properties may influence deposition of hydrates to the pipeline wall. The surface properties that are considered as the most important are wettability, surface free energy, roughness and surface charge. The surface properties may be inter-related; e.g. a surface with a high surface free energy is most likely water-wet.

3.1   Wettability

For solid surfaces and particles in contact with crude oil and water, the wettability of the system is influenced by adsorption of crude oil components giving wettability states ranging from water- to oil-wet [22]. The wettability of a solid can be quantified by the angle θ in the three-phase contact point of a liquid drop in thermal equilibrium with a horizontal surface. The contact angle θ is defined here as the angle measured through the aqueous phase. Three-phase systems are illustrated in Figures 3.1 and 3.2.

The relationship between interfacial tension and contact angle was established by Young [23] and is generally known as Young's equation

Figure 3.1: Water-wet system: A water (buffer) drop resting on a glass surface in model oil (petroleum ether). Picture acquired during laboratory experiments by the author.

Figure 3.2: Oil-wet system: A water (buffer) drop resting on a brass surface in model oil (petroleum ether). Picture acquired during laboratory experiments by the author.

$$cos\theta = \frac{\gamma_{so} - \gamma_{sw}}{\gamma_{wo}}$$ (3.1)

where γ represents the interfacial tensions between the three different interfaces: solid/oil, solid/water and water/oil. Young's equation may also represent a solid/liquid/vapor system. The transition from water-wet to oil-wet surfaces is gradual, and traditionally surfaces with contact angles lower than 75 degrees are considered as water-wet (Figure 3.1), whereas angles larger than 115 degrees correspond to oil-wet surfaces (Figure 3.2) [24]. For the intermediate angles, the surfaces have preference for neither liquid phase.

Two reviews of various techniques for determination of wettability are available from Cuicec [25] and Anderson [24]. The sessile drop technique [26] is most widespread. Modifications of the sessile drop technique and other techniques include the dual-drop dual crystal (DDDC) method [27, 28], the two-plate method [29], the Wilhelmy plate technique [30–32] and capillary rise [33, 34].

The angle determination is often based on visual determination of the three phase contact point, which can suffer from some degree of subjectivity. Complete profile edge-detection can be used to overcome the dependence of the three phase contact point in contact angle determination [35]. Axisymmetric drop shape analysis (ADSA) methods are powerful because of their accuracy, simplicity and versatility [36] and are based on the Laplace equation of capillary pressure. Two different methods have been modified by Rio et al. [36]. The axisymmetrical drop shape analysis - profile (ADSA-P), first introduced by Rotenberg et al. [37], is based on the droplet profile and difference in density between the two liquid phases involved. The axisymmetrical drop shape analysis - diameter (ADSA-D), first introduced by Skinner et al. [38], is based on the volume and diameter of a sessile drop, where the

interfacial tensions of the two liquid phases are known.

Until recently, direct measurements in systems where crude oil constitutes the bulk medium has not been possible; a transparent medium is required. Hence, investigating crude oil systems, the crude oil is mainly used for aging the substrate, and then replaced by transparent probe oil when the contact angle is to be quantified. The underlying assumption is that the replacement does not disturb the adsorbed layer of crude oil components at the solid surface [30–32, 39–44]. A second alternative has been to invert the system, depositing an oil drop underneath a solid in the bulk brine phase [45–52]. Capillary rise has also been used for determination of contact angles in crude oil systems [33, 35]. Recently, Askvik et al. [53] used the ADSA-D method to measure the angle based on the observation that a water drop in crude oil is readily detectable through the container wall from underneath. However, this method is very sensitive to errors in drop radius and particularly in drop volume [53]; the method can only be used when the solid is transparent (i.e. only on glass).

The adhesion energy may be calculated from rewriting Young's equation (3.1) into the Young-Dupré equation [54]:

$$W_{swo} = \gamma_{wo}(1 + cos\theta) \tag{3.2}$$

The adhesion energy, W_{swo}, gives the adhesion energy per unit area of a solid surface (s) and water (w) adhering in oil (o), thus it combines both interfacial tension, γ_{wo}, between the brine and oil phase (Section 4.4) and contact angle, θ, into one parameter.

3.2 Surface free energy

Surface free energy of a solid surface gives a direct measure of intermolecular interactions at interfaces and has strong influence on wetting, adsorption and adhesion behavior [55, 56]. The surface free energy is influenced by chemical composition, roughness, structure, temperature, and potentially also other factors [56].

Lugscheider et al. [57] determined the surface free energy of some metals and concluded that general adhesion increases with higher surface free energy of the solid metals. Materials with low surface free energy, such as epoxy coated surfaces, reduce wax deposition [58]. Metal surfaces are often high-energy surface similar to glass due to the well-developed oxide surface layer [57].

Sharma et al. [59] have written a very thorough review paper on different methods for determining surface free energy of solids by the use of contact angle measurements. A short summary will be presented here. The Young equation, equation 3.1, contains only two measurable quantities, the contact angle (θ) and the liquid-vapor surface tension (γ_{lv}). In order to determine the solid surface tension, γ_{sv}, an additional relationship relating these quantities has to be derived. To determine the surface free energy of solid surfaces, fluids which have a higher surface tension than the solid should be used, as illustrated in Figure 3.3 [60]. The figure plots $\gamma_{lv}cos\theta$ versus γ_{lv} for a poly(ethylene terephatalate) (PET) surface. Liquids with surface tension that is higher than the anticipated PET surface tension ($\gamma_{lv} > \gamma_{sv}$) reaches a global maximum. When the liquids has lower surface tension than the solid surface tension ($\gamma_{lv} < \gamma_{sv}$), the liquids either spread or assume very small angles on the surface and should not be used in determining the surface free energy [60].
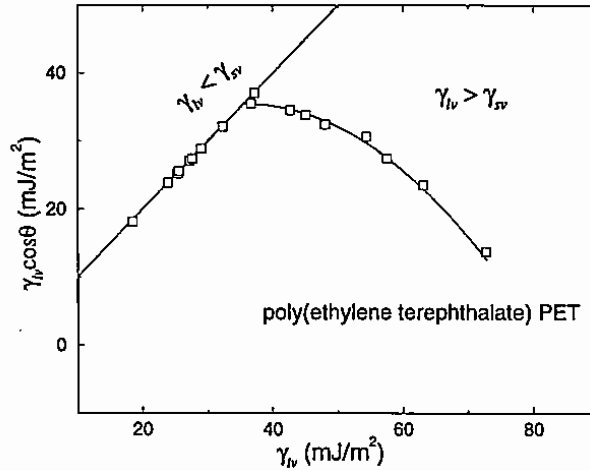
Figure 3.3: $\gamma_{lv}cos\theta$ versus γ_{lv} for a PET surface. Figure from Kwok et al. [60].

For highly energetic surfaces, there are only a limited number of liquids that can be used to determine the surface free energy. The determination of surface free energy utilizes some basic assumptions, such as no interaction between the air and solid surface and that the air is assumed to be equivalent to vacuum. The determination also assumes that there is no chemical reaction between solid and probe fluid.

In the 60s and 70s, Fowkes [61,62] pioneered with a surface free component approach, proposing that the surface free energy consists of two components, a dispersive component and a non-dispersive (polar) component, giving information about the acid-base behavior of the surfaces. However, Fowkes [61] only included the dispersive component in his relation for solid-liquid interaction. Application of the original method by Fowkes was quite restricted, and it has since been further developed by different research groups, giving several different approaches. The Owens-Wendt geometric mean approach [63], the Wu harmonic mean approach [64] and the van Oss acid-base approach [65] are

16

all based on the Fowkes approach. By using these methods, one can obtain contributions from the two components giving information about acid-base properties of the surfaces. All these approaches require at least two or three liquids of known surface tension components.

The equation of state approach, Section 3.2.1, is the method used in this work and only requires one probe liquid.

3.2.1 Equation of state for interfacial tension approach

The "equation of state (EOS) for interfacial tension" approach was first introduced by Neumann et al. [66–68]:

$$\gamma_{sl} = \gamma_{lv} + \gamma_{sv} - 2\sqrt{\gamma_{lv}\gamma_{sv}}e^{-\beta(\gamma_{lv}-\gamma_{sv})^2} \tag{3.3}$$

where β is a constant that has been determined empirically and has an average value of 0.0001247 $(mJ/m^2)^{-2}$ [68]. If this equation is combined with the Young equation (3.1), the following relation is obtained:

$$cos\theta = -1 + 2\sqrt{\frac{\gamma_{sv}}{\gamma_{lv}}}e^{-\beta(\gamma_{lv}-\gamma_{sv})^2} \tag{3.4}$$

Recently Kwok and Neumann [69, 70] modified the equation and the new equation of state for interfacial tension is as follows

$$\gamma_{sl} = \gamma_{lv} + \gamma_{sv} - 2\sqrt{\gamma_{lv}\gamma_{sv}}(1 - \beta_1(\gamma_{lv} - \gamma_{sv})^2) \tag{3.5}$$

where $\beta_1 = 0.0001057$ mJ/m^2. Combining equation 3.5 with the Young equation (3.1), the following relation is obtained:

$$cos\theta = -1 + 2\sqrt{\frac{\gamma_{sv}}{\gamma_{lv}}}(1 - \beta_1(\gamma_{sv} - \gamma_{lv})^2) \tag{3.6}$$

Only one liquid with known surface tension, γ_{lv}, is needed to determine the surface free energy, γ_{sv}, of a solid surface, but neither the dispersive nor the polar component can be evaluated.

It is a basic assumption of the EOS approach that the surface free energy of the solid is independent of the probe fluid. This assumption is based on extensive experimental data, mainly from the group of Neumann [66–68]. Further work has shown that the independence of the probe fluid is not always strictly true, but that deviations are small [71–73].

3.3 Roughness

Surface roughness plays an important role in adhesion, since it changes the contact area between the bodies involved and leads to a change in interaction. There are several applications that use surface roughness to control or change adhesion. Some of the technical applications that use roughness to control adhesion are the medical industry (in cell adhesion either to improve cell adhesion in bone growth or to reduce bacterial adhesion [74–78]), the shipping-industry (in relation to reduction in biofouling [79,80]) and improvement of printing quality [81].

The strength of dry adhesion of small particles on rough surfaces is mainly determined by the geometric effects of the surface-particle system [82]. Reduction in contact area between two bodies caused by changes in surface roughness is suggested to lead to reduction in interaction and adhesion [82–84]. Under wet conditions, however, the adhesion has been found to both increase [85] and decrease [86] with increasing surface roughness. Jorda [87] found an increase in wax deposition with increase in roughness of steel pipeline surfaces. Liquid bridging is a crucial factor for adhesion to

be strong on very rough surfaces. However, the surface area is not always directly proportional to the surface roughness [88].

Some parameters that may be used to describe surface roughness are average roughness, R_a, maximum height, R_t, and surface index, r_{si}. R_a represents the average height of individual points in the surface, calculated over the entire measured area, given by the equation

$$R_a = \frac{1}{n} \sum_{i=1}^{n} \left| Z_i - \bar{Z} \right| \tag{3.7}$$

where n is the number of points measured, $\bar{Z}$ is the average height of the entire region and Z_i is the height of each individual point. The maximum height, R_t, represents the vertical distance between the highest and lowest points in the evaluated area. The surface index is a measure of total surface area compared to the lateral (two dimensional) surface area. An ideally smooth surface will have a surface index of 1, whereas a rough surface will have a surface index > 1.

3.4 Wettability and surface roughness

A liquid drop that is placed on a clean, planar and smooth solid surface, resides on the solid surface with the contact angle, θ_e, defined by Young's equation 3.1. For real surfaces, there are two main effects that may change this angle:

- physical heterogeneity, such as roughness

- chemical heterogeneity, such as mixed chemical surfaces

Volpe et al. [89,90] previously stated that wettability is a combined property of chemical composition and surface roughness. A value of the contact

angle is relatively easy to obtain from a flat and homogeneous surface, but it is not as straight-forward on very rough and/or heterogeneous surfaces [90]. The roughness may strongly influence the contact angles [89].

Young's equation and deviations thereof, are only valid for perfectly smooth surfaces, which are never fulfilled in real systems. No single contact angle can characterize a surface. A maximum advancing angle and a minimum receding angle are observed, with a range of metastable angles observed in between these boundaries. When inflating a drop (Figure 3.4 a), the contact angle, θ, can exceed θ_e without the contact line moving at all. When θ reaches a threshold value, θ_a, the three phase contact line finally does move [91]. θ_a is referred to as the advancing angle. When deflating a drop (Figure 3.4 b), θ can decrease down to a limiting value, θ_r, known as the receding angle [91].
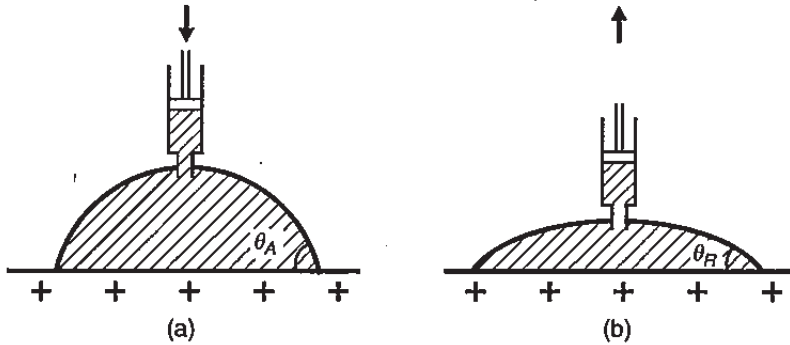
Figure 3.4: (a) Advancing angle, θ_a, when the drop is inflated; (b) receding angle, θ_r, when drop is deflated. Figure from de Gennes et al. [91].

The contact angle hysteresis ($\triangle\theta$) is referred to as the difference between the limiting angles θ_a and θ_r. The contact angle hysteresis ($\triangle\theta$) can vary as much as 50° (or 90° [92]), but on a well-prepared smooth surface, the

difference θ_a - θ_r is very small ($< 5°$) [91]. As the roughness increases, the magnitude of the hysteresis increases and goes through a maximum before decreasing suddenly [93, 94], as shown in Figure 3.5.
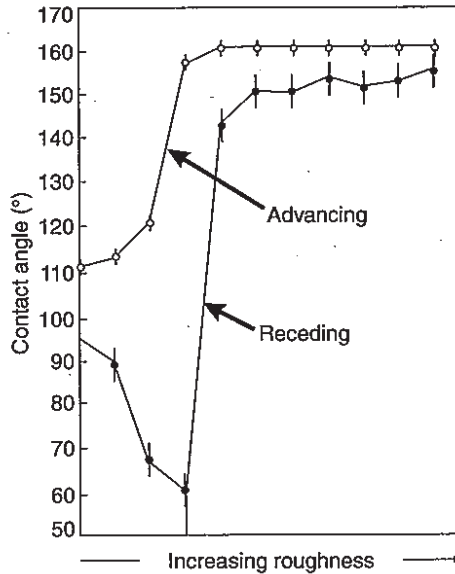
Figure 3.5: Advancing and receding angles of water drops on wax surfaces as a function of roughness of the substrate. Figure from de Gennes et al. [91] adapted from Johnson et al. [93].

The magnitude of the hysteresis is determined by balance between vibrational energy of the drop and the height of the energy barriers [94]. In order to be sure that roughness effects on contact angles of liquids on polymers can be excluded, surface roughness, R_a, of the solid surface should be less than 0.1 μm [92, 95]. Advancing and receding contact angles are both examples of dynamic contact angles, where the angle is determined while the droplet is moving (inflating or deflating). A static contact angle is a contact angle obtained from a droplet resting on a solid surface and is neither the advancing

nor receding angle, but somewhere within the hysteresis range. The advantage of a static contact angle is that only one value is produced, however it does not give any indication of influence of roughness on the measured angle and may be less reproducible. The method used in this work is the static sessile drop method (Papers I-V). This method produces a semi-advancing static angle where a drop is deposited onto the solid surface and the droplet is briefly advancing on the surface before it rests. Several parallels (8-12) are performed to exclude outliers and assure reproducible results.

It has been proposed that surface roughness can be used to control the degree of wettability (for a given surface chemistry) by enhancing the material's natural tendency. As the roughness increases, a hydrophilic substance becomes even more hydrophilic, while an initially hydrophobic surface can become "super-hydrophobic" (see Figure 3.6). Enhancement of the natural wetting properties with increased roughness may be a bit controversial, since the advancing angle increases with increasing roughness and the receding angle decreases with increasing roughness [92], independent of initial wetting properties.

Wetting models have been developed for rough surfaces (Wenzel and Kamusewitz) and heterogeneous surfaces (Cassie-Baxter).

3.4.1   Wenzel's model

For Wenzel's model to be applicable, the roughness scale has to be much smaller than the size of the droplet [91, 96]. According to Myers [97], the relationship between a theoretical contact angle (i.e. for a completely smooth surface) and the actual surface angle is given by

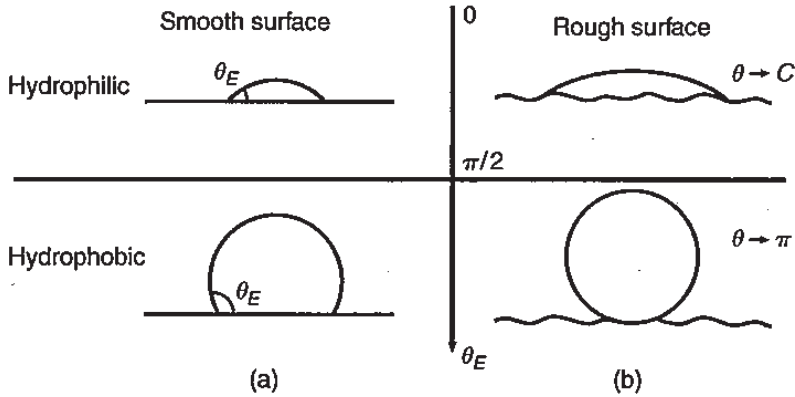$$r_w = \frac{cos\theta_{exp}}{cos\theta_w} \tag{3.8}$$

Figure 3.6: Controlling the wettability of a substrate through its roughness. (a) Smooth surface; (b) rough surface. Hydrophilic substrate becoming even more hydrophilic with a rough surface (top); hydrophobic substrate becoming "super-hydrophobic" (bottom). Figure from [91].

where r_w is the roughness factor (usually termed as Wenzel's roughness factor) that represents the ratio of the true area of the solid to the apparent area of the surface; i.e. two-dimensional area for a corresponding surface without any roughness. A roughness factor of 1 ($r_w = 1$) represents a completely smooth surface whereas a roughness factor larger than 1 ($r_w > 1$) represents a rough surface.

Neumann et al. [92] states that the theoretical contact angle determined in Wenzel's equation is not a Young contact angle and should not be inserted into the Young equation (3.1) and equations derived thereof.

3.4.2 Kamusewitz model

Another method to account for surface roughness has been proposed by Kamusewitz [98], where changes in contact angle hysteresis ($\triangle\theta$) have been used to obtain an ideal contact angle for smooth surfaces. The barrier effect states

that the advancing angle (θ_a) increases by the same amount as the receding angle (θ_r) decreases, given by the arithmetic mean with the corresponding Young angle, θ_e [98]

$$\theta_e = 0.5(\theta_a + \theta_r) \tag{3.9}$$

However, experiments have shown that the relationship is not always an arithmetic mean of θ_a and θ_r, but must be represented by individual slopes A_a (advancing) and A_r (receding) dependent on the system under investigation [98]

$$\theta_e = \theta_{exp} - A_n\Delta\theta \tag{3.10}$$

where A_n is the slope of the line (correlating $\Delta\theta$ and θ_{exp}) and $\Delta\theta$ is the contact angle hysteresis. This is illustrated in Figure 3.7, where the contact angle hysteresis ($\Delta\theta$) is plotted against the advancing (θ_a, wetting) and receding (θ_r, dewetting) contact angles for the system paraffin wax/water/vapor. The situation in this system is close to, but not exactly, an arithmetic mean of the advancing (θ_a) and receding (θ_r) contact angles.

The Kamusewitz model indicates that either the receding angle or advancing angle measured on rough surfaces of varying degree can be used to extrapolate to an angle measured on a perfectly smooth surface. As previously stated, a smooth surface will not have contact angle hysteresis [91].
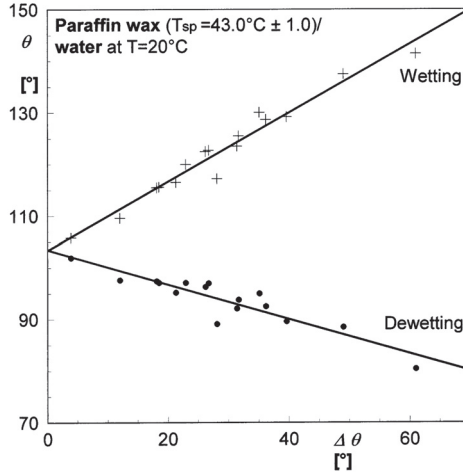
Figure 3.7: Advancing (wetting) and receding (dewetting) contact angles versus the hysteresis for the system paraffin wax/water at 20 °C. Figure from Kamusewitz et al. [98].

3.5 Surface charge and reactivity

All the metal surfaces investigated in this work are covered with an oxide layer [99]. A summary of the composition and the surface layers used in this work are presented in Table 6.1 and in Paper II. The type of oxides present on the surface layers influence the behavior and reactivity.

Carboxylic acids or naphthenic acids (see section 4.3), which are the most common acids in crude oils [16], have strong chemical interactions with metals. The metal oxide on the surface may react with carboxylic acids as shown for an aluminum surface in Figure 3.8. The proton originally associated with the free acid head group (-COOH) reacts with either certain Al-O sites to form a surface hydroxyl or with an existing surface hydroxyl (Al-OH) to form water [100, 101].

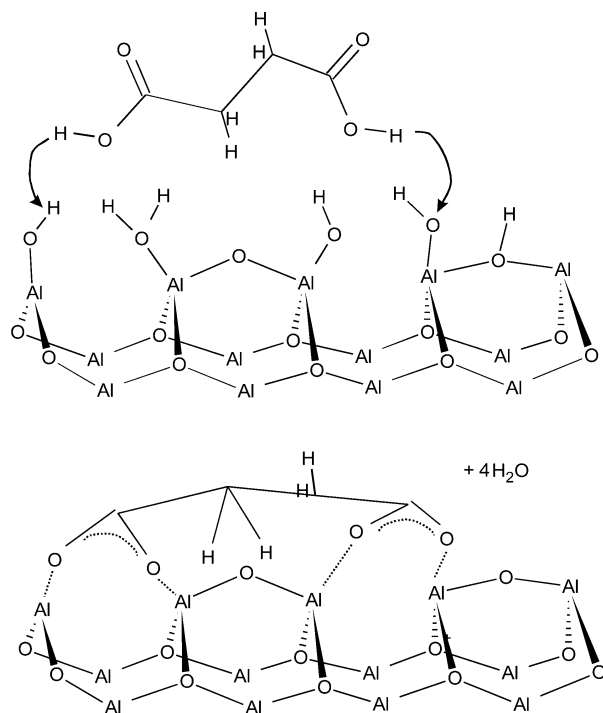The adsorption of carboxylic acids forming a SAM (self-assembled mono-

Figure 3.8: Illustration of chemisorption of bifunctional carboxylic acid on aluminum oxide surface through the removal of hydroxyls on the oxide surface [101].

layer) is believed to be driven by a Lewis Brønsted type acid-base chemistry between the reactive carboxylic acid head and specific surface reactive sites by chemisorption [100–109]. Monolayer adsorption can be thought of as a site filling procedure. Increasing stability of the monolayer will be achieved as the hydrocarbon chain length of the carboxylic acid increases [107] and with an increasing number of carboxylic groups on the carboxylic acid [101, 102].

The difference in reactivity for different surfaces can be understood by investigating surface charge, which is dependent on pH of the water phase described in Section 3.5.1 and general theory from inorganic chemistry on reactivity of metals compared to non-metals, as discussed in Section 3.5.2.

3.5.1 Surface Charge

Solid oxides in aqueous suspension are generally electrically charged. An understanding of surface charge is important in studying the chemistry of corrosion, wettability and adhesion [110]. The electric charge is dependent on the pH of the aqueous phase. The pH that results in zero net charge of the surface is called the isoelectric point (IEP) or point of zero charge (PZC). PZC refers to the absence of any type of surface charge, while IEP refers to the state of neutral surface charge; i.e. if positive and negative charges are both present in equal amounts. IEP and PZC for solid surfaces are identical by definition [111]. The term PZC will be used from here on. Contact angle measurements are very dependent on surface charge and can be used for determination of PZC [112, 113]. Contact angles go through a maximum at the PZC of oxide surfaces [112].

Metal oxides will hydrolyze in the presence of water to form hydroxide layers at the surface (M-OH). At pH values above the PZC, the surface will be negatively charged (Equation 3.11) and will act as an acid. At pH values

below the PZC, the surface will be positively charged (Equation 3.12) and the surface will act as a base. The surface reaction that may occur depending on the pH may be written as:

$$M - OH = M - O^- + H^+(aq) \qquad (3.11)$$

$$M - OH + H^+(aq) = M - OH_2^+ \qquad (3.12)$$
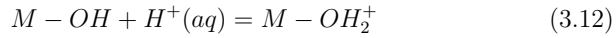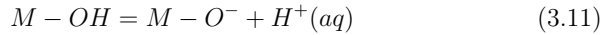
The M denotes the surface element present in the surface oxide layer. Decreasing the pH leads to an increase in positive charge, whereas increasing the pH reduces the positive charge and the surface charge may become negative.

Table 3.1 list the average PZC values, determined at room temperature (25 °C) for some of the most common oxides. The list is adapted from Kosmulski [114] and references therein. The values are based on the average of several published values. A value for stainless steel has also been included, adapted from Kallay et al. [115]. A large number of values have been reported for aluminum oxide, iron oxide and silicon oxide, but only a few measurements have been determined for chromium oxide, zinc oxide and copper oxide.

As seen from Table 3.1, most of the metal oxides have PZC in the pH range 8-10. Chromium oxide deviates a bit from the other metal oxides with a lower PZC in the range 5-9. This is most likely the reason why stainless steel (with a PZC of 4.7) is used to prevent corrosion due to the formation of a protective Cr_2O_3 surface layer. SiO_2 has a much lower PZC compared to the metal oxides and will behave differently in most pH ranges.

Table 3.1: Average point of zero charge (PZC) for some of the most common oxides at room temperature (≈ 25 °C).

Oxide	point of zero charge, PZC (pH)
Al_2O_3	8.6 (average) [114]
Fe_2O_3	7.5 (average) [114]
SiO_2	2.3 (average) [114]
$Cr_2O_3/Cr(OH)_3$	5.5/8.6 [114]
ZnO	9.1 (average) [114]
CuO	9.5 [111]
Stainless steel (316)	4.7 (average) [115]

3.5.2 Reaction of metals versus non-metals

Three different types of elements exist:

- Metals (such as Al, Fe, Cr, Cu and Zn)

- Metalloids (such as Si)

- Non-metals (such as C, N and O)

Reactivity will be dependent on the types of elements that are present on the surface. Metals will exist as metal oxides and silica as a metalloid. Glass mainly consists of silicon oxide (SiO_2), with varying amount of impurities, such as borate (BO_3^{-3}); quartz is the purest form of SiO_2. Epoxy consists of carbon (C), nitrogen (N), oxygen (O) and hydrogen (H), as shown in Section 3.6 and will behave as a non-metal.

Metalloids, such as SiO_2, tend to have physical properties that are similar to metals, but chemical properties that are similar to non-metals.

While metals form basic oxides, non-metals form acidic oxides. Since metalloids have chemical properties similar to the non-metals, metalloids will form acidic oxides. The interaction between a basic surface (metal oxides) and acidic carboxylic acids will be stronger than with an acidic surface (glass and epoxy).

3.6   Epoxy coating

Epoxy polymers are easy to process; are very safe; have excellent moisture, solvent and chemical resistance; are tough; have low shrinkage on curing; good electrical, mechanical and corrosion resistance; and have excellent adhesion to many substrates [116,117]. Epoxy resins have been widely used as surface coatings, adhesives, painting materials, potting laminates, encapsulants for semiconductors, polymer composites, and insulating materials for electronic devices, etc. [116,117]. There are numerous paint/coating systems based on epoxy resin available for corrosion and biofouling prevention, for use in, for instance, marine activities. These fields of application are constantly under improvement due to unsatisfactory behavior with regard to corrosion. Epoxy is also used as an inner surface coating in gas pipelines [118]. Epoxy is suggested as an efficient coating in preventing wax deposition due to low surface free energy [58].

The epoxy consists of two parts which are mixed shortly before use. The main component of part A is a diepoxy molecule group containing two so-called epoxy-groups (Figure 3.9 A), while the main component of Part B is a diamine (Figure 3.9 B). When the two substances are mixed, a cross linked network is created as shown in Figure 3.10, resulting in a hard substance that can be very strong. The chemical reaction is irreversible.
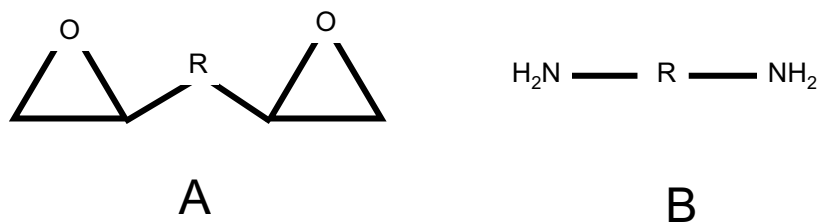
Figure 3.9: The two main components of the epoxy coating. A) A diepoxy molecule that contains two diepoxy groups. B) A diamine molecule containing two amine groups, NH_2.
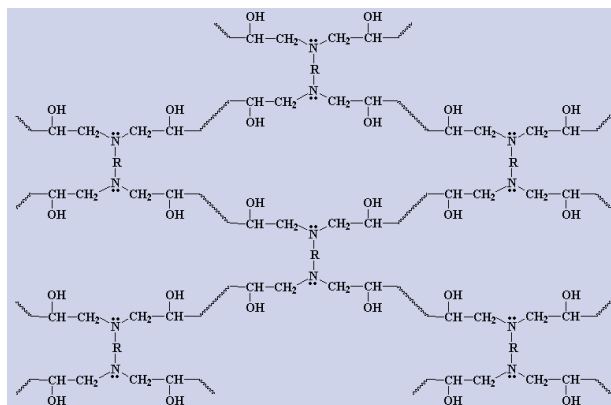

Figure 3.10: The epoxy resin consistent in the epoxy surface resulting in a cross linked network which is a hard substance that can be very strong. Figure from internet page [119].

Chapter 4

Crude oil and its influence on wettability

Crude oils are complex mixtures consisting of a wide range of highly complex chemical compounds, such as alkanes, aromatics, cycloalkanes, resins and asphaltenes. Crude oil composition is dependent on many factors, such as its place of origin, the age of the field and the temperature it has been stored at in the ground. The main elements in crude oil are carbon and hydrogen, with small amounts of nitrogen, oxygen, sulfur and metals [16].

Biodegradation is microbial alteration of crude oil. Bacteria are, under some subsurface conditions, able to degrade some of the compounds present in crude oil, using them as a source of carbon [120]. Biodegradation results in reduction of the crude oil quality and economic value. The enrichment of heavy polar components leads to an increase in density, viscosity, acidity and content of sulfur, asphaltenes and metals [121–124]. Biodegraded oils have higher total acid and total base contents [125].

4.1 Wettability of solid surfaces

The effect of crude oil on wettability has been studied widely, e.g. [33, 35, 40, 45, 46, 48, 52, 53], though most contact angle studies have been performed on glass and not directly measured in the crude oil because a transparent medium is required for determining the angle. Glass is often used as a model for reservoir rock in research related to recovery of crude oil from reservoirs and is therefore a surface that is thoroughly studied. Glass is, most likely, not an appropriate model for pipeline surfaces. Some studies have also been performed on metal surfaces [52, 126]. Glass surfaces are more prone to display water-wet behavior, due to their strongly hydrophilic behavior, compared to pipeline steel surfaces [52].

Because of their surface-active properties, the polar components of the oil are pointed out as the main species responsible for alteration of surface wettability trough interaction of their polar functional groups with the surface polar sites [40, 45, 127–130]. Asphaltenes and resins are the most polar oil fractions and contain the highest amounts of surface active species [24, 39, 127, 128, 131–137]. It is also suggested that the acids are agents influencing the surface wettability [30, 45, 46, 136], where acid-base interactions are the main mechanisms [33, 40, 41, 138]. Bases have also been suggested to change wettability [45, 136, 138]. Buckley et al. [138] have suggested that oils with either a high ratio of bases to acids or the opposite, a high ratio of acids to bases, have recognizable tendencies to alter wetting. dos Santos et al. [52] found that both removal of asphaltenes and naphthenic acids reduced the contact angle for steel surfaces from an oil-wet behavior to a water-wet situation.

Wetting of a substrate and adhesion of crude oil is also very dependent on the pH of the water phase [39–41, 45–47, 53, 127, 136, 137, 139–141], aging

time and temperature [40, 42, 141].

4.2 Wettability of hydrates

Crude oils have varying potentials for forming hydrate plugs, indicating that some oils contain natural compounds that act as anti-agglomerants [7]. Anti-agglomerants are surface-active and are able to adsorb to the hydrate surface (as illustrated in Figure 4.1) and presumably also to the pipeline surface, creating oil-wet surfaces. This reduces the possibility for hydrogen-bonding and may reduce agglomeration or deposition. The formation of oil-wet hydrates correlates with non-agglomerating behavior and low hydrate plugging tendency [8]. Several authors [8–12, 142] have suggested that the inhibiting components are contained within the acid fraction of the crude oil. Borgund et al. [11] observed that the amount of phenolic compounds found in the acid extracts have a strong negative correlation with agglomeration/plugging effect. Erstad et al. [12] suggested that the type of acid present is more important than the total amount of acids present in the crude oil. The non-plugging oils have relatively higher amounts of weakly polar compounds and ester carbonyl functionalities, while the plugging oils have relatively larger amounts of polyfunctional compounds [12].

Asserson [143] recently developed a method for performing contact angle measurements on Freon hydrates, however the method was challenging and time-consuming due to low quality of the hydrate surface and low reproducibility. Addition of acids extracted from crude oils made the hydrate surface more oil-wet [143]. Addition of various modified crude oils has also been shown to influence the adhesion force between hydrate particles [144], presumably due to adsorption of surface active components present in crude
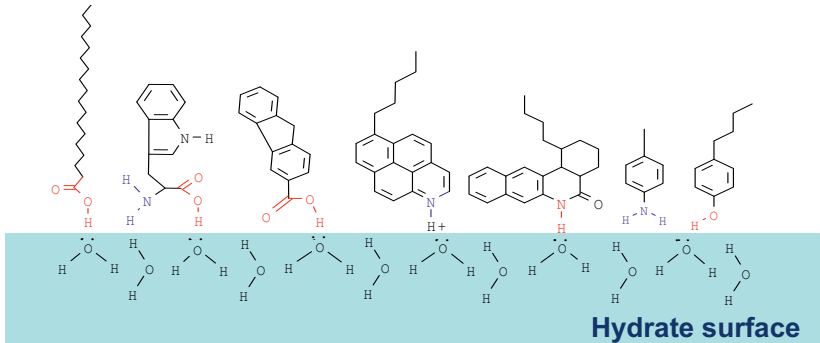
Figure 4.1: Surface active components in crude oils can adsorb to hydrate surfaces and change the wettability which reduces the agglomeration of hydrate particles (Adapted by courtesy of Sylvi Høiland).

oils. Unmodified crude oils had a stronger influence on the adhesion forces compared to deasphalted and acid extracted oil [144]. The wetting properties of hydrate particles have also been shown to influence emulsion properties of oil/water/hydrate systems, as discussed in Section 4.2.1.

4.2.1 Hydrate wetting index

Høiland et al. [8] have developed a procedure to determine the indigenous hydrate plugging tendencies for crude oils based on emulsion behavior. Solid particles, such as hydrate particles, present at the interface between two phases in an emulsion of a water/oil system, may obtain various wettability states depending on the oil/water/solid interfacial tensions of the system. The wetting state of the particles is dependent on the chemical composition of the crude oil; i.e. the presence of components in the crude oil that have an affinity for the solid hydrate surface [8]. The wetting state of the solid particles will determine whether they stabilize water-in-oil emulsions (oil-wet particle surfaces) or oil-in-water emulsions (water-wet particle surfaces)

[145,146]. An illustration of how the wetting of a hydrate particle can change emulsion properties is shown in Figure 4.2. Oil-wet particles will reside in the oil phase (left) and stabilize water-in-oil emulsions (oil-continuous), whereas water-wet particles will reside in the water phase and tend to stabilize oil-in-water emulsions (water-continuous). Depending on the liquid fractions of oil and water, the emulsion will either be an oil-continuous or water-continuous emulsion. The inversion point will depend on the wetting state of the emulsion-stabilizing particles. The inversion point of a particle-stabilized emulsion system can be determined by changing the ratio of oil to water [147].
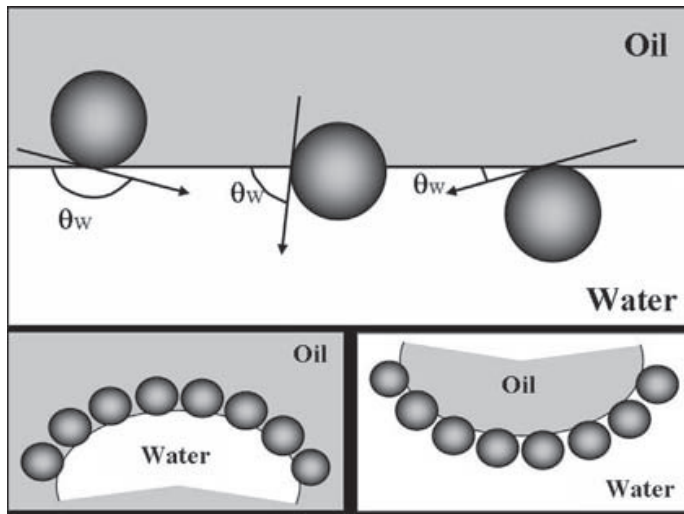
Figure 4.2: Illustration of a hydrate particle residing at an oil-water interface. Oil-wet particles (contact angle > 90°) will reside in the oil phase (left), and tend to stabilize water-in-oil emulsions. Water-wet particles (contact angle < 90°) will reside in the water phase (right), and tend to stabilize oil-in-water emulsions. Figure from Høiland et al. [8].

The point of phase inversion is found for both systems with hydrates and

without hydrates for the same oil. The difference between the phase inversion points (with hydrates - without hydrates) is represented by a scale from -1 to +1. Negative values and values close to zero indicate that the oil produces water-wet or intermediate-wet hydrates. Positive values indicate that the oil produces oil-wet hydrates. This method is used to differentiate oils with regard to plugging tendency.

It has been shown, from using multivariate data analysis, that the plugging tendency can be predicted fairly well by combining four compositional parameters: biodegradation level, asphaltene content, TAN value and density [148]. Each compositional parameter has a different weighting, meaning that the different compositional features have difference importance toward the plugging tendency.

4.3 Petroleum acids

Acids influence the interfacial activity of the crude oils [149–153]. Acids are formed due to biodegradation process [121, 154, 155]; normally, highly biodegraded oils contain a larger amount of acids [125].

The acid fraction tested in this thesis is a commercial naphthenic acid. Commercial naphthenic acids are extracted from crude oils [156] and comprise a large part of the petroleum carboxylic acids. The naphthenic acids are a complex mixture of alkyl substituted acyclic and cycloaliphatic carboxylic acids. The acids can be represented by the general formula $C_nH_{2n+Z}O_2$, where n denotes the number of carbon atoms and Z specifies the hydrogen deficiency, see Figure 4.3. When Z is 0, the formula represents an acyclic fatty acid, i.e. acids with a saturated hydrocarbon structure. More information about naphthenic acids can be found in a review article by Clemente

and Fedorak [156] and references therein.

$CH_3(CH_2)_mCO_2H$

Z = 0

R—⬠—$(CH_2)_mCO_2H$ R—⬡—$(CH_2)_mCO_2H$

Z = − 2

R—⬡⬠—$(CH_2)_mCO_2H$ R—⬡⬡—$(CH_2)_mCO_2H$

R—⬠⬠—$(CH_2)_mCO_2H$

Z = − 4

R—⬠⬡⬠—$(CH_2)_mCO_2H$ R—⬡⬡⬡—$(CH_2)_mCO_2H$

R—⬡⬠⬠—$(CH_2)_mCO_2H$

Z = − 6
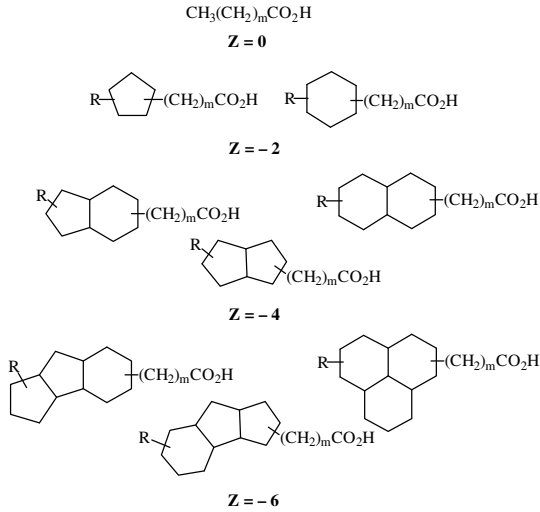
Figure 4.3: Naphthenic acid structures where R is an alkyl chain, Z describes the hydrogen deficiency and m is the number of CH_2 units, from Clemente and Fedorak [156].

4.4 Interfacial tension

Interfacial tension can be defined as the free energy change in expanding the interfacial area between two immiscible liquids in contact by one unit area [54]. As mentioned above, interfacial tension is influenced by surface active components, such as acids [149–153]. Low average molecular weight carboxylic acids adsorb at interfaces, reducing the oil-water interfacial tension which also leads to emulsion stabilization [157]. The presence of long aliphatic chains, together with the carboxylic acid groups, account for the ability of a crude oil sample to reduce the interfacial tension [157].

It has been suggested that the tendency to form hydrate plugs increases as the surface activity decreases [7]. The relationship between interfacial tension and plugging potential is still not necessarily straight-forward [7].

The liquid-liquid and air-liquid interfacial tensions, γ, can be measured by the drop weight method [110], using Harkins-Brown equation [158]

$$\gamma = \frac{(V \Delta \rho g)}{(2 \pi r F)} \qquad (4.1)$$

where V is the drop volume, $\Delta \rho$ is the difference in density of the two phases, g is the acceleration due to gravity ($g = 9.81 \ m/s^2$), r is the radius of the needle and F is a correction factor which is based on the radius of the needle and the volume of the droplet. Figure 4.4 shows the experimental set-up used to determine interfacial tension. The average volume of ten droplets is used to determine the interfacial tension between two phases.
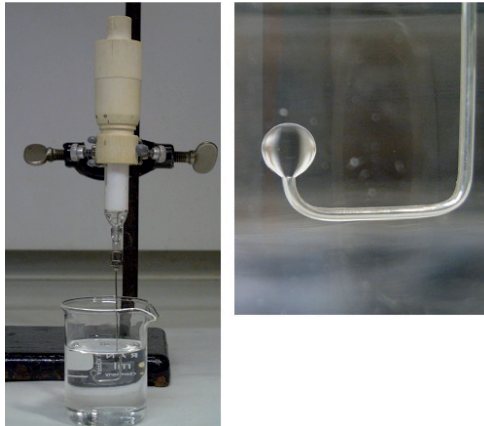

Figure 4.4: Experimental set-up for the droplet-weight method, where the needle of a micrometer syringe is dipped into the bulk of another (left). A liquid drop is formed at the tip of the needle (right). The volume is registered manually from the scale on the upper part of the needle. Picture from the master thesis of Asserson [143].

4.5   Near infrared spectroscopy

Spectroscopic analysis of crude oil with NIR light is a technique recently applied to characterize the oil; i.e. measuring the content of main groups in the crude oil [159–162].

In this work, the main purpose of using a NIR system is to be able to obtain pictures of water droplets in crude oils to determine the contact angle, as illustrated in Figure 4.5. Aakre et al. [163] have used a NIR technique to investigate crude oil emulsion images where the crude oils are transparent to light. The full NIR region is approximately between 800 nm and 2500 nm. In the present work, the region used is 800 to 1700 nm.
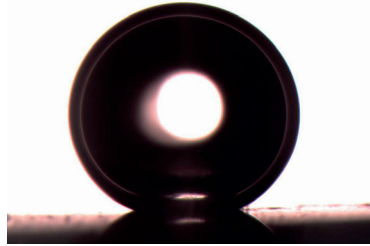
Figure 4.5: A water drop deposited on a stainless steel surface in black crude oil. Picture acquired during laboratory experiments by the author. (Figure 2, Paper IV).

NIR spectra of the crude oils used in this work are shown in Figure 4.6. These spectra were used to determine the degree of transparency and where the oils are most transparent. The spectra show that the oils are most transparent in the region from 1200 to 1650 nm. The oils have varying degree of transparency. Only 10 of the 20 oils in the NIR-spectrum were chosen to be used in the contact angle experiments. The oils that were selected had varying compositional features and were among the most transparent crude

oils (with lower optical density), compared to some of the oils that were considered as not transparent enough for the initial camera set-up. The aqueous buffer used in these experiments is also included in this spectrum (red dashed line), and it is seen that the buffer has different transparency than the crude oils at most of the wavelengths in the infrared region. The set-up used for obtaining contact angle images from water droplets in crude oils is illustrated in Paper IV, Figure 4.
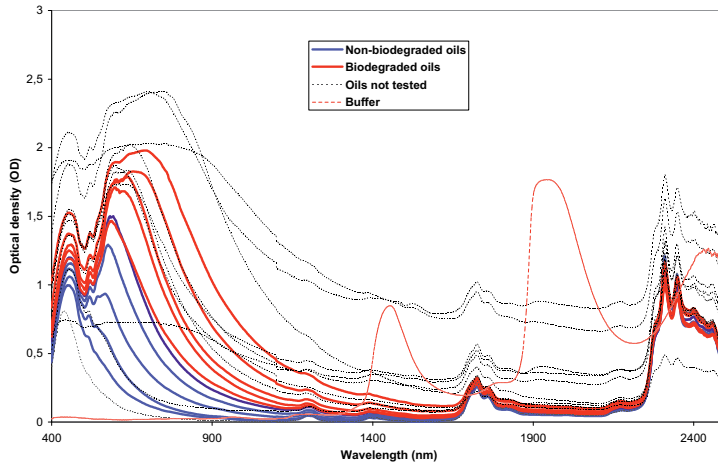
Figure 4.6: Near infrared spectrum of the crude oils. The wavelength region where the crude oils are most transparent is between 1200 and 1650 nm. The oils used in the contact angle measurements are shown in solid blue and red lines, indicating which are biodegraded (red) and non-biodegraded (blue). The buffer is represented by the red dashed line. The oils not used in the contact angle measurements are also shown with black dashed lines.

It was also seen that there is a correlation between optical density and asphaltene content (Figure 5, Paper IV). Crude oils with a high content of asphaltenes have a higher optical density and are therefore less transparent.

Chapter 5

Deposition mechanisms

Particle adhesion and deposition is a carefully studied subject and several review articles and books have been published on the topic [164–169]. Several publications are related to particle deposition from flowing suspensions [166–173].

Yang et al. [170] have performed an extensive theoretical analysis on particle deposition. The deposition process has been conceptually divided into four stages, depending on the separation distance between the particle and the wall:

1. At large distances from the wall, the motion of the particles is influenced by convection and migration due to external forces, such as gravity.

2. At distances comparable to the particle size, particle-wall hydrodynamic interactions are controlling. Hydrodynamic drag on the particle, because of the stationary wall, influences the particles' movement.

3. At closer distances (1-100 nm), DLVO interactions, which include van der Waals forces and electrostatic forces/electrical double layer (EDL), are the most significant.

4. At distances within 0.5-1.0 nm, the so-called primary energy minimum (PEM), stochastic effects such as flux due to discrete surface charges at the wall and particle surface, surface heterogeneity and roughness etc., may play pronounced roles.

In this thesis, the focus will be on distances within 0-100 nm, where the surface properties in static systems are the main issue, as well as the effect of an oil phase on the surface properties. The shape of the interaction energy profile, which is the sum of the strength of the van der Waal interaction field and EDL, has strong influence on particle deposition [170, 171]. Chein et al. [171] found that particles can be suspended above or deposit onto the wall, depending on the Hamaker constant (a constant that reflects the surface potential of the phases involved) and the thickness of the EDL. The distance where adhesion influence from the wall commence cannot be calculated from theoretical considerations [171] and is usually approximated as a constant (Krupp [174] and Israelachvili [54] have suggested the values 0.4 nm and 0.2 nm, respectively).

5.1 General adhesion forces

Adhesion can be defined as the free energy change to separate unit areas of two media 1 and 2 from contact to infinity in vacuum [54]. Particle adhesion is defined by particle-particle interactions and is influenced by material properties, particle size and shape, surface properties, external load, temperature, humidity and electrostatic charges [175]. Some of these influences are dependent on the system under investigation.

Adhesion forces between particles can be divided into three types: van der Waals forces, electrostatic forces and capillary forces. Van der Waals and

electrostatic forces are the basis of the DLVO theory; in humid conditions or when a liquid bridge occurs between particle and surface, capillary action also occur. The DLVO theory was established by Derjaguin and Landau [176] and by Vervey and Overbeek [177] and explains colloidal stability. The sum of the DLVO forces can either be repulsive or attractive depending on the Hamaker constant, particle size, charges of the particle, wall and suspension medium and separation distance [171]. In aqueous media, interfaces are almost always charged, due to adsorption of ionic surface active molecules or dissociation of ionisable surface sites [170]. Adamczyk et al. [166] have reviewed electrostatic interactions and found that large deposition occurs when the ionic strength in the system is high and when the flow rates are low. Capillary forces have been given some attention in this thesis, since they seem to be the main contribution in hydrate agglomeration and deposition.

5.2   Capillary forces

When a particle deposits onto a solid, capillary forces can act between the particle and solid, if a liquid bridge is present. The nature of the interactions between a particle and a surface is strongly modified by the liquid meniscus that forms between the surfaces at humid conditions [54]. The additional force between a particle and the surface arising from the formation of the meniscus of a liquid bridge is defined as the capillary force [54]. The capillary force can easily be the dominant interaction in such systems [178]. The capillary force is dependent on the ambient humidity and hydrophobicity of both the solid surface and the particle [179].

The capillary force arises as a consequence of the suction pressure (termed the Laplace pressure) caused by the curvature of the liquid interface between

water and oil (or gas) [5], given by the Young-Laplace equation

$$P_{cap} = \gamma_{ll} \left(\frac{1}{r_1} + \frac{1}{r_2} \right) \approx \frac{\gamma_{ll}}{r_1} \; (since \; r_2 >> r_1) \tag{5.1}$$

where γ_{ll} is the interfacial tension between the two liquid phases involved, and r_1 is the principle radii of curvature of the particle surface, as illustrated in Figure 5.1, and r_2 is the principle radii of curvature of the solid surface, which may be assumed as infinitially large.
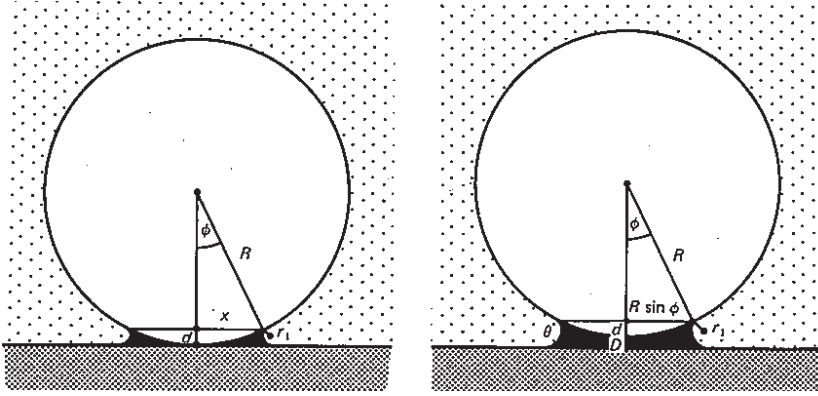
Figure 5.1: Schematic of liquid bridge between a particle and a solid surface with different separation (D) between them. Figure from Israelachvili [54].

The capillary force of the capillary bridge between a solid and a particle can be determined by the contribution of the LaPlace pressure (shown in Figure 5.1), which is given by [54]

$$\frac{F_{cap}}{R^*} = \frac{2\pi\gamma_{ll}cos\theta}{1 + D/2d} \tag{5.2}$$

where γ_{ll} is the liquid-liquid interfacial tension and θ is the contact angle of the capillary liquid on the solid particle, D is the height of the liquid bridge, d is the height of the wetting on the particle and R^* is the harmonic

mean radius, as given in equation 5.4. Maximum attractive force is between the particle and surface when $D = 0$ (Figure 5.1 (left)), so $\frac{D}{2d} << 1$.

5.2.1 Capillary bridging in hydrate agglomeration and deposition

Camargo and Palermo [180] suggested that hydrate agglomeration in oil systems is dominated by capillary attractive forces; the attractive forces between two hydrate particles estimated from DLVO forces were an order of magnitude below experimental observations. The concept of capillary force between hydrate particles and between hydrate particles and pipeline walls has been investigated by Sloan and co-workers [181–184]. It is indicated that adhesion force decreases with increasing sub-cooling (i.e. increasing degrees below freezing point), due to loss of quasi-liquid layer on the particle surface. The strength of the liquid bridge is mainly controlled by two forces: capillary forces and viscous forces [5]. The low viscosity of water makes capillary forces dominant over viscous for water bridges in hydrate agglomeration [5].

The use of dry hydrate particles has been suggested to considerably reduce hydrate particles from agglomerating [6, 185–191].

5.3 Measuring adhesion forces

A number of techniques have been developed in particle technology for investigating particle-particle or particle-surface adhesion, for example, optical tweezers [192], micropipette aspiration [193, 194], atomic force microscopy [195, 196] and micromechanical force apparatus [86, 181, 197, 198]. In an attempt to remove particles from surfaces, one generally uses gravitational forces, centrifugal forces, flowing forces and mechanical forces. Although

these forces also increase with the particle diameter, they decrease much faster than the adhesive forces with increasing particle size. Therefore, smaller particles can adhere to a surface with greater strength.

5.3.1 Hydrate adhesion forces

As mentioned, Camargo et al. [180] indicated that capillary attraction dominates hydrate agglomeration in the oil phase and that subsequent freezing of the necks strengthens the hydrate plug.

Fan et al. [197] have shown, with micromanipulation, that the adhesion force between ice particles increases with their size and contact time. The adhesion forces decrease as the temperature is reduced from the freezing point for particles of ice or hydrates, i.e. with increasing subcooling [181]. The amount of liquid at the particle-particle contact should increase with temperature, increasing the bridging area and therefore increasing the adhesion force [181]. At temperatures near the melting point, a disordered quasi-liquid layer can exist on a solid surface, a phenomenon called surface melting. There is a high degree of variation in reported results, which is most likely due to surface roughness [181]. Nicholas et al. [4] measured adhesion forces between cyclopentane hydrates and carbon steel surfaces, concluding that the adhesion force is much lower than between two hydrate particles. When a water drop is deposited between the hydrate and the carbon steel surface, the hydrate cannot be detached from the solid surface; this indicates that there are very strong capillary forces present [4].

5.3.2 Micromechanical force apparatus

A micromechanical force (MMF) apparatus designed for measuring hydrate-hydrate and hydrate-solid adhesion forces was originally developed by Yang

et al. [181]. Detailed information about the technique can be found elsewhere for hydrate-hydrate adhesion forces [86, 198] and for solid-hydrate adhesion forces [199]. In this thesis, cyclopentane (CyC5) was chosen as a suitable hydrate former (see Section 2.4). A CyC5 hydrate is shown in Figure 5.2, which illustrates particle sizes and their surface roughness.
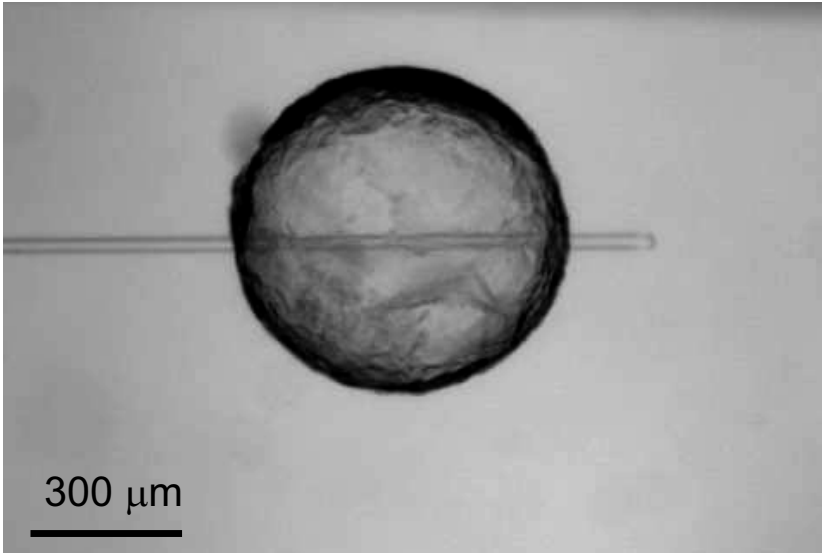
Figure 5.2: A cyclopentane hydrate particle on a glass fiber cantilever. The figure is from the PhD thesis of J. Nicholas [199].

The adhesive force, F_{adh}, is calculated from using Hooke's law

$$F_{adh} = k\delta \tag{5.3}$$

where k is the spring constant of the cylindrical glass fiber and δ is the displacement required to separate the two particles [200]. More details on determination of the spring constant can be found in the master thesis by Taylor [86]. The adhesion force is normalized by the harmonic mean radius

to account for different particle sizes. The harmonic mean radius, R^*, is given by the following equation

$$\frac{1}{R^*} = \frac{1}{2}\left(\frac{1}{R_1} + \frac{1}{R_2}\right) \tag{5.4}$$

where R_1 and R_2 are the radius of the particles under investigation. The radius of solid samples is considered to be infinite. The set-up used to determine the adhesion force between cyclopentane (CyC5) hydrates and solid surfaces is illustrated in Figure 5.3. The left cantilever holding the hydrate particle is a stationary cantilever that can be operated by hand. The right cantilever holding the surface sample is a high precision micromanipulator that is operated remotely.
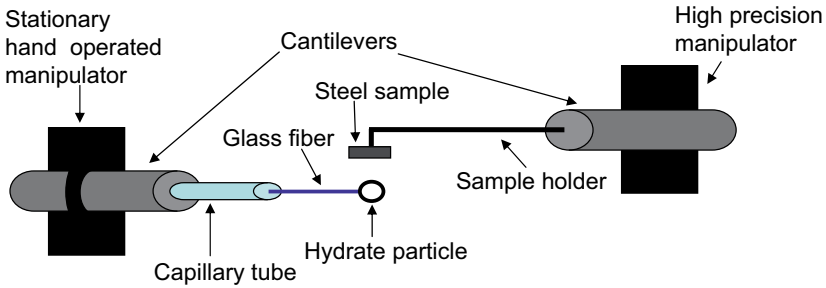
Figure 5.3: Micromechanical experiment with a hydrate particle and a solid surface. The figure is adapted from the PhD thesis of J. Nicholas [199].

The solid surface cantilevers used in the MMF experiments are shown in Figure 5.4.
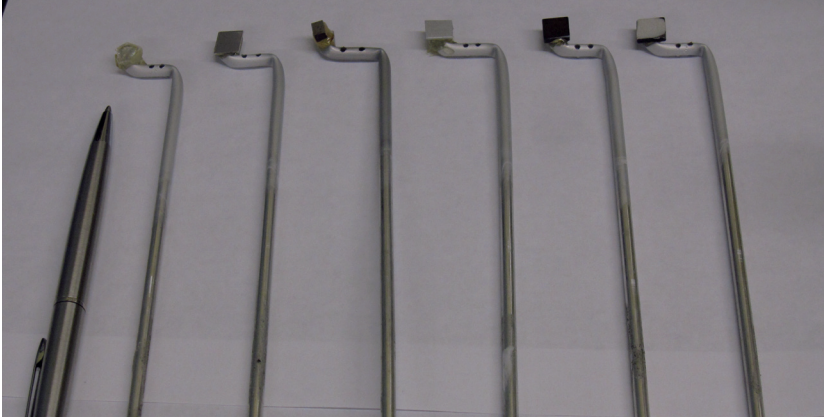
Figure 5.4: The solid surface cantilevers used in the micromechanical force experiments. The cantilevers are sorted according to surface free energy left to right: glass, stainless steel, carbon steel, aluminum, brass and epoxy.

5.4 Influence of flow

Fluid flow has a strong influence on the probability of hydrate deposition. Kosinski et al. [201] have estimated the probability of particle deposition in terms of particle diameter (a) and initial particle velocity ($|v_y^{(0)}|$) prior to collision, with computational numerical simulations, as shown in Figure 5.5. Hamaker forces and friction forces are taken into account, however, the model refers to a single particle only and no consideration has been given to capillary forces. It is shown that deposition increases with a decrease in initial velocities and particle diameters.

Fluid flow regimes can be quantified through the dimensionless Reynolds number (Re), which is dependent on four variables: velocity (N), pipeline diameter (D_{pipe}), density (ρ) and viscosity (μ).

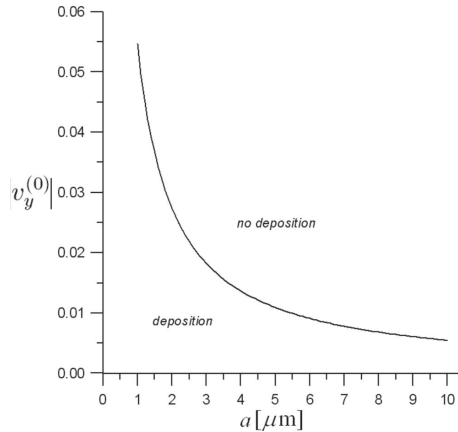$$Re = \frac{N D_{pipe}^2 \rho}{\mu} \tag{5.5}$$

Figure 5.5: Initial particle velocity prior to wall collision ($|v_y^{(0)}|$) versus particle diameter determined by computational numerical simulations. Figure from Kosinski et al. [201].

The type of flow experienced in the pipeline, which can be either laminar or turbulent, is dependent on the Reynolds number, as discussed in the master theses by Pedersen [202] and Kilinc [203]. With Reynolds numbers below 2000, laminar flow is experienced; with Reynolds numbers above 4000, turbulent flow is experienced [204]. There is a transition region between these two boundaries (Re 2000-4000). Laminar flow does not exert any lateral mixing on the fluid, whereas turbulent flow is highly disordered; i.e. the fluid elements move randomly in three dimensions.

Liquid droplets are deformed by flow as shown in Figure 5.6, producing receding and advancing angles. The forces required to detach the droplet are dependent on the contact angle (apparent contact area) and temperature [205, 206]. These forces increase with decreasing contact angle [205, 206] and decreasing temperature [206].

Figure 5.7 illustrates an air bubble in a water phase before "lift-off" (no
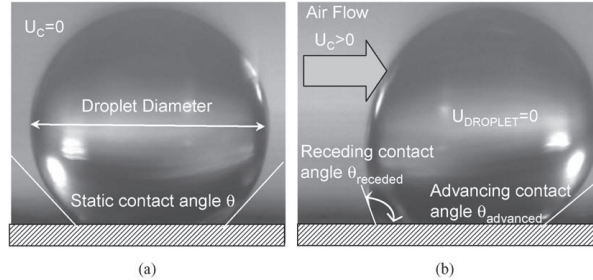
Figure 5.6: (a) Static contact angle of a non-moving liquid drop. (b) Contact angle of a non-moving liquid drop influenced by air flow resulting in dynamic advancing and receding angle. Figure from Theodorakakos et al. [206].

flow experienced). Figure 5.7 (a) and (c) is prior to "lift off", whereas Figure 5.7 (b) and (d) is at "lift off". It is assumed that the contact angles θ_1 are the same at "lift off" (Figure 5.7 (b) and (d)) as in quiescent state (Figure 5.7 (a) and (c)) [207]. Hiemenz et al. [207] claim that if $\theta_1 < 90°$ (Figure 5.7 (a) and (b)), the drop is likely to leave a residue, whereas if $\theta_1 > 90°$ (Figure 5.7 (c) and (d)) would lead to a clean detachment. Similar behavior can be expected in adhesion force experiments (Section 6.3) and detachment experiments with flow (Section 6.4).

5.4.1 Gas versus oil dominated system

There exist two distinctly different systems for transport of petroleum products: gas dominated pipelines and oil dominated pipelines. Liquid loadings and flow regimes are considerably different for these two types of systems, which most likely influence the degree of hydrate plugging and deposition. Plugging in oil-dominated systems is suggested to be a product of agglomerating hydrate particles than eventually grow sufficiently large to stop the flow [13]. Hydrate formation and plugging in gas-dominated systems has
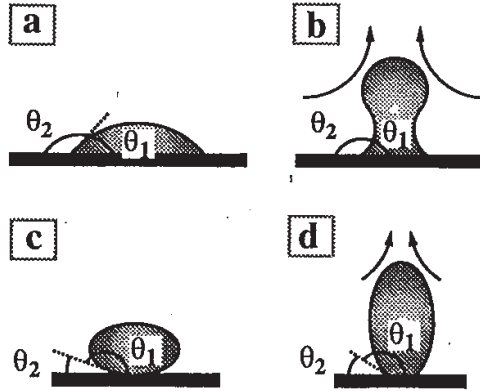
Figure 5.7: Illustration of an air bubble in flotation. (a) $\theta_1 < 90°$ prior to "lift off" (b) $\theta_1 < 90°$ at "lift off" (c) $\theta_1 > 90°$ prior to "lift off" (d) $\theta_1 > 90°$ at "lift off". Figure from Hiemenz et al. [207].

been suggested to be a product of pipeline deposition [13, 184, 208, 209]. The plugging in these systems are attributed to a release and jamming mechanism [184], as described in section 5.5.

5.5   Wall growth leading to plugging

Hydrate deposition may occur either as hydrate formation in the bulk phase and subsequent deposition on the pipe wall, or as annular hydrate formation on the pipeline wall [199].

Lingelem et al. [208] originally proposed a plugging mechanism from pipeline deposition in gas systems, as shown in Figure 5.8 which is a model extended by Sloan et al. [13]. Hydrate formation is suggested to start at the pipeline walls via vapor deposition and/or splashing water with subsequent conversions (Figure 5.8 A and B). The wall is the radial point of lowest temperature, and consequently the point of hydrate deposition due to heat

transfer with the outside environment, which is at a lower temperature than the gas [13]. As the hydrate layer grows, it will act as an insulating layer and the effective wall heat flux will be reduced [208]. For this reason, the growth of the hydrate layer will slow down at a given location as the hydrate layer thickens. The hydrate growth will in this way increase into the pipeline as the wall temperature continue to decrease [208]. Further growth leads to narrowing of the flow channel and collapse and sloughing of the deposit when it reaches a critical mass (Figure 5.8 C, D, E). The sloughed particles travel downstream to eventually plug the pipeline (Figure 5.8 F).
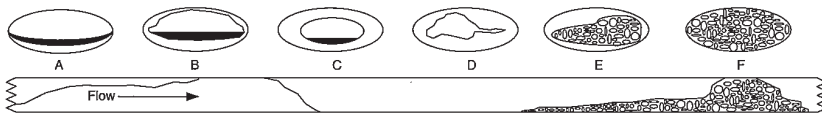
Figure 5.8: Hydrate plug formation in a gas-dominated pipelines. Figure from Sloan et al. [13] adapted from Lingelem et al. [208].

Nicholas et al. [3] simplified the process into three stages, as illustrated in Figure 5.9:

1. Wall growth; i.e. hydrates start to build up on the pipeline wall.

2. Sloughing; i.e. the deposit reaches a critical mass and collapses, hence are removed from the wall in large hydrate aggregates.

3. Plugging; i.e. the hydrate aggregates are transported with the flow and may lead to jamming further down the pipeline.

Guariguata [210] found that jamming is dependent on particle size and fixed amount of particles. Large amounts of particles and larger particle sizes will increase the probability of jamming. The ratio of pipeline diameter or diameter of open flow path (D_{pipe}) to particle diameter (a) determines
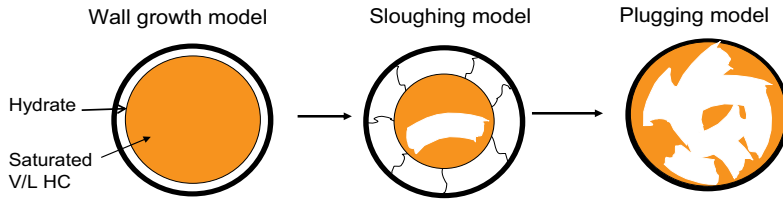
Figure 5.9: Diagram of the three steps that occur once wall growth begins. Figure from Nicholas et al. [3].

the jamming probability. Jamming occurs if $\frac{D_{pipe}}{a} < 3.2$, and will not occur if $\frac{D_{pipe}}{a} > 4.4$ [210]. Guariguata [210] found that an increase in adhesion between particles increased the jamming probability.

Another anticipated scenario of pipeline plugging as a result from wall growth could be build-up of a surface layer that eventually blocks the pipeline flow.

Chapter 6

Main Results

6.1 Surface characterization

The solid surfaces that have been investigated in the present work are stainless steel (AISI 316 L), aluminum (EN AW 5052), brass (63% Cu, 37% Zn), glass and an epoxy coating, which are shown in Figure 6.1. The epoxy coating was applied in three different ways, giving surfaces with different degrees of roughness: named Epoxy-A, Epoxy-B and Epoxy-C. A description of how these three different surfaces were created is summarized in paper III. A carbon steel surface was also tested in the micromechanical adhesion force measurements and the main surface characterization and treatment is summarized in the PhD-thesis of J.W. Nicholas [199].

The surface composition of the solids used was given by the supplier and verified from x-ray element analysis. Images from Scanning Electron Microscopy (SEM) are shown in Figure 6.2 for stainless steel, aluminum and brass. Metals such as iron, nickel, zinc, aluminum and copper are covered by layers of oxides which have been produced by adsorption of additional oxygen from the atmosphere and diffusion processes in the layer [57,99]. The
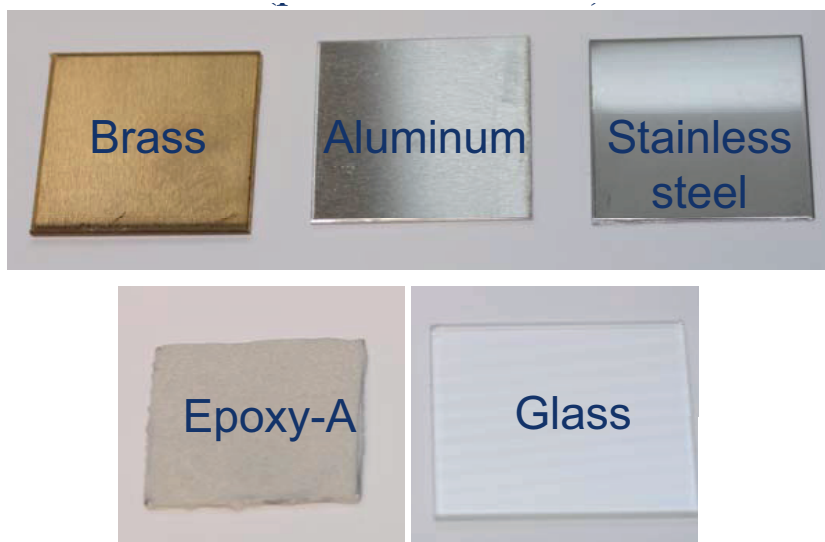
Figure 6.1: The surfaces used in the experimental work. The surfaces used are brass, aluminum, stainless steel, epoxy-coated surfaces and optical glass. These pieces with size of approximately 3x3 cm were used in the model oil experiments. Smaller samples (approximately 1x1 cm) were used in the crude oil and MMF experiments.

main components and surface layers characteristics are summarized in Table 6.1.

Surface free energies and roughness factors for the solid surfaces are summarized in Table 6.2. The surface free energies for the solids range from 33 to 65 mJ/m^2. For glass, only one probe fluid could be used. Therefore, the value for glass is given without a standard deviation, although the uncertainty for measurements on glass is probably similar to those for the other materials. The values obtained fall within the range of previously reported values of surface free energies, which range from 30 to 50 mJ/m^2 for different metal surfaces when using contact angle measurements and probe fluids [56,57,211].

The three surfaces Epoxy-A, Epoxy-B and Epoxy-C are assumed to be
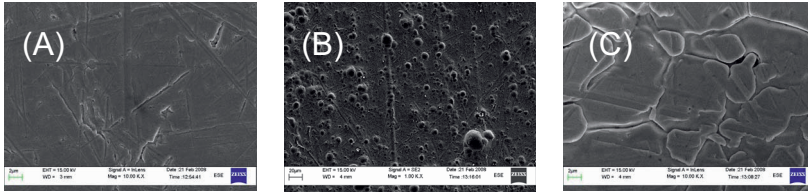
Figure 6.2: Images from Scanning Electron Microscopy (SEM). (A) Brass (B) Aluminum (C) Stainless steel. These images illustrate how different the surfaces are on a microscopically level.

Table 6.1: Components in solids used in this work and the main surface layer composition. Further discussion can be found in Paper II.

Solid surface	Components	Main surface layer
Glass	SiO_2, Trace: Borate	SiO_2
Stainless steel	≈ 68 % Fe, 18 % Cr, 12 % Ni, 2 % Ni Trace: C, Si	Cr_2O_3 / $Cr(OH)_3$ Trace Fe_2O_3
Carbon steel	≈ 98 % Fe Trace: 0.3-1.7 % C	Fe_2O_3
Aluminum	≈ 96 % Al, 2 % Mg Trace (0.1-0.5 %): Si, Fe, Cu, Mn, Zn	Al_2O_3
Brass	63 % Cu, 37 % Zn	CuO, ZnO
Epoxy	Main comp.: Epoxy-group containing molecule and diamine	See Figure 3.10

of the same initial chemical composition, but they are quite different with respect to their average roughness, R_a, ranging from 8 to 16 μm, as given in Table 6.2. The surface roughness increases going from Epoxy-A to Epoxy-B to Epoxy-C. Even though the roughness for all the epoxy coated surfaces is relatively different, the maximum height, R_t (vertical distance from highest and lowest point), is in the same order of magnitude ranging from 146 to 178 μm.

The surface index indicates that the total surface area is not proportional to the surface roughness, which was previously indicated by Donoso et al. [88].

Table 6.2: Surface characterization of the solid surfaces used in this work

Solid surface	Surface free energy* γ_s(mJ/m^2)	Average roughness R_a (μm)	Maximum height R_t (μm)	Surface index r_{si}
Glass	65	0.01	0.34	-
Stainless steel	64 ± 5	0.13	6.86	-
Carbon steel	61 ± 5	-	-	-
Aluminum	59 ± 1	0.48	12.26	-
Brass	47 ± 5	0.34	3.13	-
Epoxy-C	-	15.80	178	1.071
Epoxy-B	-	11.12	146	1.049
Epoxy-A	33 ± 1	8.31	158	1.248

* It is assumed that the surfaces used for determination are ideally smooth. The SFE of the Epoxy-A surface are most likely more influenced by roughness compared to the other surfaces.

Epoxy-A has the largest effective surface area, even though it has the lowest average roughness. When the roughness of the solid surface is less than 0.1 μm, surface roughness effects on contact angles can be excluded [95]. Since the surface roughness for the epoxy coated surfaces are much larger than this limit, the contact angles are expected to be influenced by the roughness.

6.2 Contact angle measurements and adhesion energies

The results from contact angle measurements are presented in Papers I-V. The contact angle is used to determine the adhesion energy, which is calculated from rewriting Young's equation into the Young-Dupré equation [54], Equation 3.2. Adhesion energy includes both contact angle and interfacial tension between water and oil, γ_{wo}, giving the adhesion energy between solid and water in an oil phase.

6.2.1 Model oil system

Papers I and II illustrate the results from the contact angle measurements in a model oil system, Figure 6.3. It can be seen that the contact angle increases as a function of acid concentration, creating more oil-wet surfaces, which most likely is due to adsorption of acids on the solid surfaces [30, 45, 46, 136]. The acids have different adsorption behavior on the different surfaces which can be explained by a difference in reactivity and surface charge, as discussed in Section 3.5. The metal surface will be differently charged compared to glass and epoxy due to a pH of 6 in the aqueous phase according to the theory of point of zero charge (see Section 3.5.1). This leads to a positive charge for most of the metal surfaces and a negative charge for the glass surface.
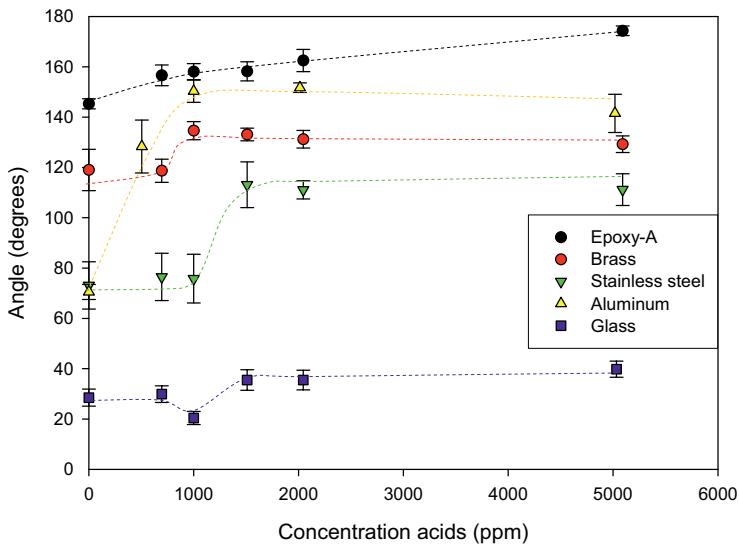
Figure 6.3: Contact angle of water drops on solid surfaces in petroleum ether with different concentrations of naphthenic acids. (Figure 3, Paper II).

The surfaces reach a limit of saturation at approximately 1000 ppm. This

may indicate that the surface experiences a monolayer adsorption that is saturated at a certain point [100–109].
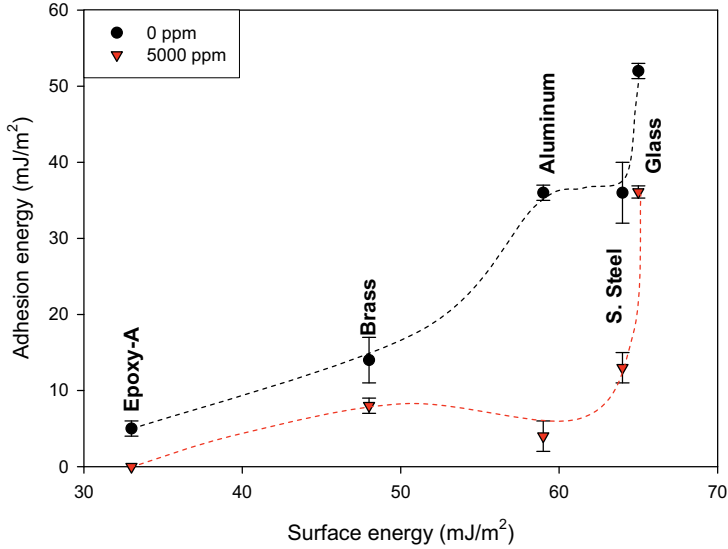
Figure 6.4: Correlation between solid surface free energy and adhesion energy of brine in petroleum ether without acids and with 5000 ppm of acids. (Figure 6, Paper II).

The adhesion energies between brine and solid in the presence of oil (Equation 3.2) decrease with increasing acid concentration (Figure 5, Paper II). The adhesion energy correlates with the solid surface free energy, shown in Figure 6.4. The adhesion of water to a solid surface in oil is lower for surfaces with low surface free energies, meaning that the aqueous phase has less tendency to stick to these surfaces. The graph also shows a decrease in adhesion energy as the concentration of acids is increased; i.e. the surfaces have become more oil-wet. The most favorable condition to reduce the adhesion force between water and solid in oil is therefore to use solid surfaces with low surface free energy and increased concentration of acids in the oil-phase.

An adhesion energy of 0 mJ/m^2 is obtained for Epoxy-A when the oil phase contains 5000 ppm of acids.

6.2.2   Influence of roughness

Since Epoxy is the surface where adhesion energy is lowest between water and solid in the presence of oil, this surface should be given specific attention. This surface is obtained by coating metal surfaces, as mentioned in Section 6.1. Creating a smooth surface is not achieved and the surfaces are therefore rougher compared to traditional metal surfaces. The influence of roughness in these surfaces was studied explicit and the results are presented in Paper III.

As introduced in section 3.4, the Young equation (3.1) and subsequent equations should not be used for non-ideal surfaces. Contact angle hysteresis will occur for rough surfaces. The roughness parameter that correlates best with the measured contact angles is the average roughness (R_a), as seen in Figure 6.5. This graph correlates average roughness (R_a) and measured contact angles for three specific acid concentrations (0, 1000 and 5000 ppm). The angles are extrapolated to zero roughness according to Kamusewitz's approach [98] (see Section 3.4.2).

It can be seen that, for a given acid concentration, an increase in average surface roughness, R_a (A<B<C, Table 6.2), leads to reduction in contact angles and less oil-wet surfaces. This indicates that an ideally smooth surface will be strongly oil-wet. Based on the extrapolation to zero roughness (Figure 6.5), an ideally smooth surface would yield a measured angle of approximately 174°.

When acids are introduced, the measured angles are increased for Epoxy-A and Epoxy-B, rendering these surfaces more oil-wet. It can seem as if the
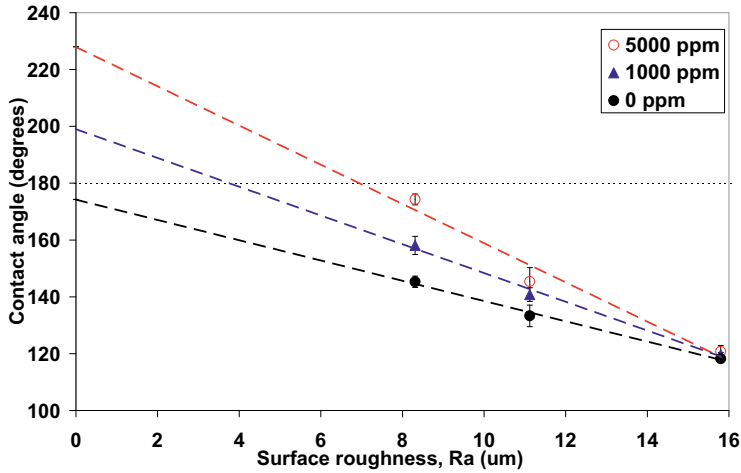
Figure 6.5: Correlation between measured contact angles of water drops on the epoxy coated surfaces with different average surface roughness, R_a. The oil phase used contained 0, 1000 and 5000 ppm of acids. (Figure 5, Paper III).

surfaces are influenced differently by the acids, which can result from steric hindrance; the carboxylic acids may be more easily ordered on a smooth surface compared to a rough surface.

Similar trends, as for 0 ppm of acids, are found for the systems with added acids (Figure 6.5). The experimental obtained contact angle (θ_{exp}) decrease with an increase in average roughness (R_a). By extrapolating the average roughness to zero, angles above 180° (more accurately 199 and 228°) are obtained. The contact angles are estimated to 180° which represents completely oil-wet and water-repelling surfaces. This is very close to the value without acids. This may indicate that smooth epoxy surfaces will be strongly water-repelling in oil-systems independent of the presence of acids.

These results indicate that surface roughness influences the measured contact angles drastically. This should be kept in mind when comparing

results for solids that may have a difference in surface roughness. From evaluation of water drops with identical volumes (see Paper III for details), it may seem as increased roughness lead to an increase in net adhesion between water and solid, and higher probability for deposition of hydrates.

6.2.3 Crude oil system

The results from crude oil systems are presented in Paper IV. Ten crude oils, with varying compositional features, were investigated (Table 1, Paper IV). Only four oils were tested on the three solids having the lowest surface free energies, since the angles measured were large ($> 150°$) and the variation between these measurements were small.

Glass behaves different from the metal surfaces. This can be due to differences in surface charge and reactivity, as discussed in Section 3.5. A general increase in measured contact angles with an increase in the surface free energy of the solid surfaces was found; i.e. more oil-wet surfaces (Figure 6.6). This is similar to the behavior found for the model oil systems.

Poor correlations between single compositional features and measured contact angles/adhesion energies illuminate the need for multivariate data analysis, as shown in Figure 6.7. There is a clear distinction between the biodegraded oils that are suggested as plugging oils from the wetting index (B1a and B5a), compared to the biodegraded oils that are considered as non-plugging (B2a, B4a, B4c). The non-biodegraded oils (marked with S), which are considered plugging oils, are also separated from the other oils.

Only the most important correlations found in the multivariate data analysis are mentioned here. There is a positive correlation between the angles measured on steel and TAN - TBN; i.e. large values in measured angles on stainless steel are found for crude oils that has a high content of excess acids
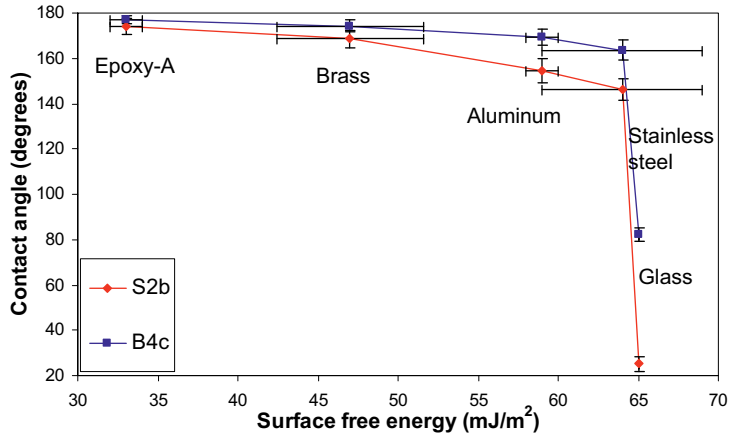
Figure 6.6: This graph illustrates how the wettability changes for different surfaces. Two crude oils, S2b and B4c, are used as examples. (Figure 5, Paper IV).

compared to bases. This is the case for the biodegraded oils in the same area (blue ring), B2a, B4a, B4c.

There is a positive correlation between the angle measured on glass and the TAN value; i.e. large values in measured angles on glass are found in the crude oils with high content of acids. This has a negative correlation to the non-biodegraded oils (green square), which has a low acid content and low measured angles on glass.

The plugging index has a positive correlation to TAN - TBN and the contact angles measured on steel (Figure 8, Paper IV); i.e., oils with a high plugging index give rise to large measured angles on steel. The plugging index has a negative correlation with the adhesion energies measured on steel, which is illustrated in Figure 6.8 with a R^2-value of 0.91; i.e. a large plugging index results in low adhesion forces between water and solid in the presence of crude oil.
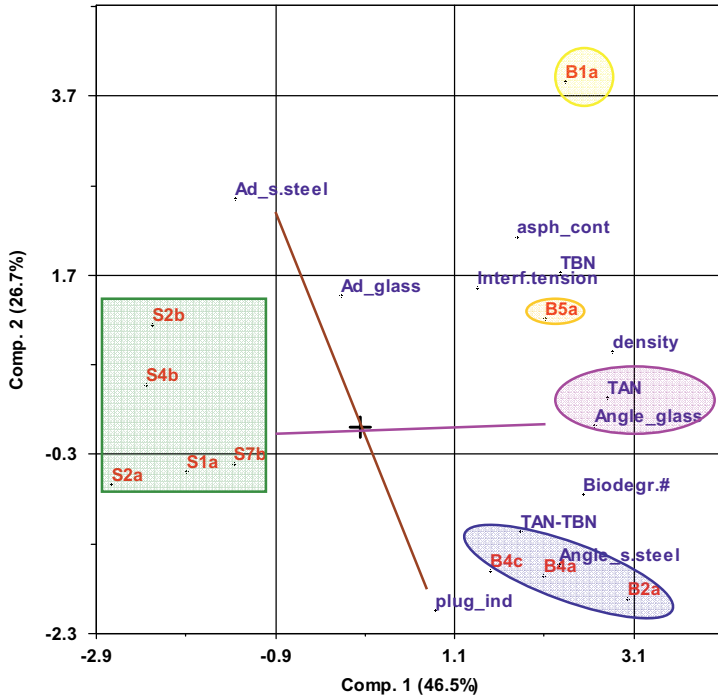
Figure 6.7: PCA plot of all crude oils (red) and variables (blue). The measured contact angles, adhesion energies and the plugging index (wettability inversion point) have been included. The non-biodegraded plugging oils are assembled (green square) while the biodegraded, non-plugging oils are assembled (blue ring). The two biodegraded plugging oils (B1a and B5a) are separated from the other biodegraded crude oils. (Figure 7, Paper IV).
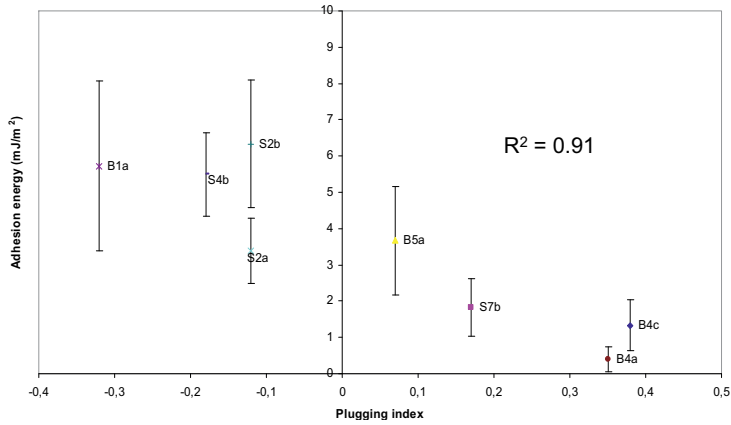
Figure 6.8: Correlation between the plugging index and adhesion energy between water and stainless steel surface in the different crude oils. (Figure 9, Paper IV).

Figure 6.8 indicates that there is a correlation between oil-wet hydrates and oil-wet pipeline surfaces, which suggests that the same components influence both hydrate and pipeline surfaces. As described above with the different correlations found in the PCA plot in Figure 6.7, both TAN and TAN-TBN have an influence on contact angles/adhesion energies. The acid fraction is highlighted as the main fraction that contains the surface active components that reduce hydrate plugging [8–12,142]. It has also been pointed out that the type of acids present is more important than the total amount of acids in the crude oil [12].

6.3 Adhesion force measurements

The micromechanical force experiment for solid surfaces and a hydrate were performed both with and without water present, in addition to experiments with petroleum acids such as naphthenic acids in the oil phase, as described

in Paper VI. The influence of the presence of acids and water on the adhesion force between hydrates was also investigated (Papers VI and VII). The experiments were performed at 3.2 °C, which corresponds to 4.5 °C subcooling for cyclopentane hydrates.

The adhesion forces for CyC5 hydrates on the different solid surfaces, characterized by their surface free energy, are shown in Figure 6.9. The adhesion force between solid and hydrate (S-H) increases with increasing surface free energy of the solids, which indicates that the initial wetting properties of pipeline surfaces may influence the deposition of hydrates to the pipeline wall.
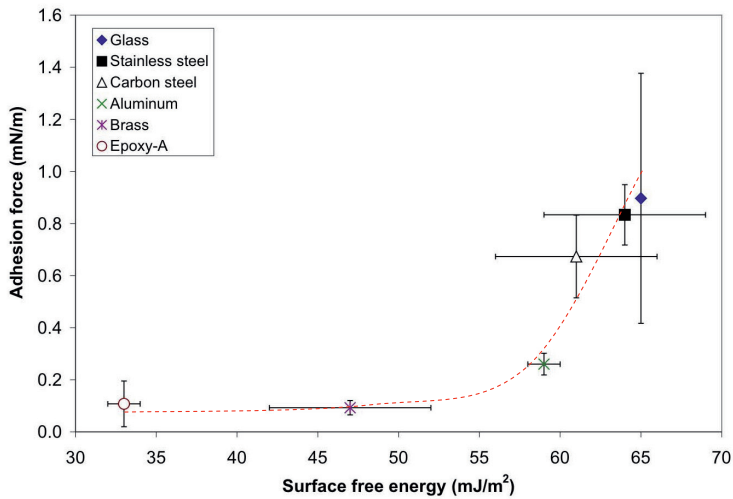
Figure 6.9: Adhesion force measurements between CyC5 hydrates and different solid surfaces at 3.2 °C (4.5 °C sub-cooling) correlated to the surface free energy of the solids. (Figure 1, Paper VI).

All measured adhesion forces determined for cyclopentane hydrates are summarized in Figure 6.10. Several different solid surface were investigated, as mentioned previously, however the values presented in Figure 6.10 are the

average value of all the forces measured for the different solids in each S-H system. The different S-H forces are the following: "dry" solids (S-H), "dry" solids with added acids (S-H acids), a water drop added to the solid surface (S-H water, also shown in Figure 6.11 A), and a droplet added to the solid surface and added acids (S-H water + acids, also shown in Figure 6.11 B). The adhesion forces between cyclopentane hydrates are for the addition of water (H-H water), the addition of acids (H-H acids), and the addition of both water and acids (H-H water + acids). The adhesion force measured for two cyclopentane hydrates is collected from the master thesis of Dieker [198].
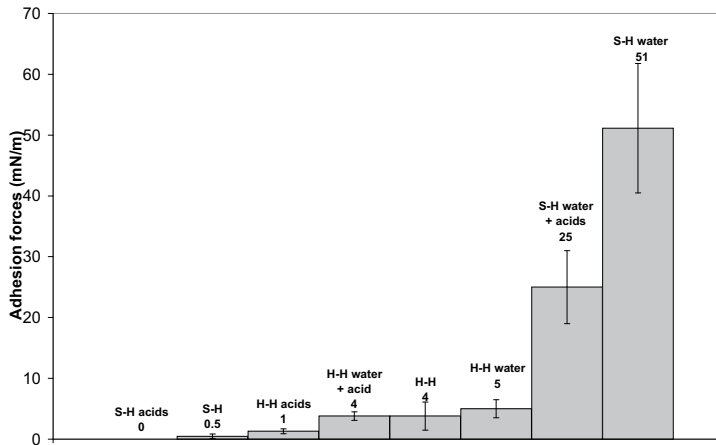
Figure 6.10: Summary of all measured adhesion forces for solid surfaces and cyclopentane hydrates at 3.2 °C (4.5 °C sub-cooling). The value for H-H adhesion forces has been collected from the master thesis of Dieker [198]. Data collected from paper VI and VII.

The forces measured for solid surfaces (S-H) are approximately 10 times lower compared to hydrate-hydrate (H-H) adhesion forces. However, when a water drop is deposited onto the solid surface (S-H water), the forces increase significantly and are approximately 10 times larger than hydrate-hydrate ad-

hesion forces (H-H). The large forces may indicate that a hydrate particle adhering to a water droplet on the pipeline wall will remain there and not be detached. Naphthenic acids reduce adhesion forces for both solid surfaces (S-H acids and S-H water + acids), and hydrates (H-H acids and H-H water + acids). The presence of water seems to have a greater influence on adhesion forces than addition of acids. Compared to other model surfactants, petroleum acids are the most effective added component except for addition of crude oil, as shown in Figure 4, Paper VII.
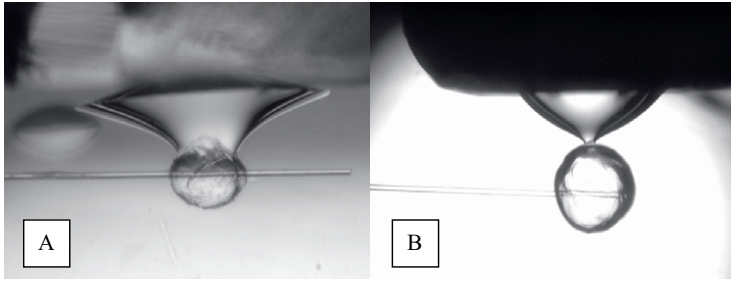
Figure 6.11: Illustrations of experiments between the solid surfaces and cyclopentane hydrates (S-H water). Acids are added to the system shown in picture B (S-H water + acids). When acids are present the water does not wet the hydrate as was seen in the systems without acids. The acids adsorbed to the hydrate surface and at the oil/water interface reduce the water from bridging to the hydrate surface.

Figure 6.11 A shows a general experimental image with a water drop deposited onto the solid. The water drop is stretched before it detaches. Some water deposits on the hydrate particle, which may subsequently convert to hydrate. The contact angle of water on the solid surfaces (as in Figure 6.11 A) corresponds to the measured adhesion force between solid and hydrate, indicating that the highest forces are obtained for the most water-wet surfaces; i.e., small water contact angle (Figure 9, Paper VI).

Figure 6.11 B shows the experimental behavior when acids are added to

the system, in addition to a water drop on the solid surface. The water does not wet the hydrate surface in a similar manner as was seen without acids (Figure 6.11 A). This suggests that the wetting properties of the hydrate surface and solid surfaces are changed due to adsorption of petroleum acids, most likely producing more oil-wet surfaces. The interfacial tension is also decreased when acids are present, leading to lower adhesion forces.

6.4 Influence of flow

A simple "stirred beaker" experimental set-up was created to study the influence of flow on detachment of water/hydrate from pipeline wall materials, as described in Paper V. The stirring rates required to detach a water droplet/hydrate particle from solid surfaces were identified. The correlation between surface free energy of the solids (Table 6.2) and the flow rates required to detach a water droplet containing hydrate former (15 % TBAB), Figure 6.12, indicate that the initial wetting properties influence the flow rate required to detach a deposited water droplet from the solid surface.

The surfaces with the highest surface free energy (glass, stainless steel and aluminum) require a higher flow rate than the surfaces with lower surface free energy (Brass and Epoxy-A). Epoxy coated surfaces require the lowest stirring rate. The water droplet could not be detached from glass with Reynolds numbers above approximately 1700 (which was the maximum speed attained with the set-up). The initial wetting properties do influence the forces required to detach a water droplet from the solid surface, which are confirmed by others [205, 206].

The experiments with a hydrate particle attached to the surface, converted from a liquid drop, indicates that hydrates will not be detached from
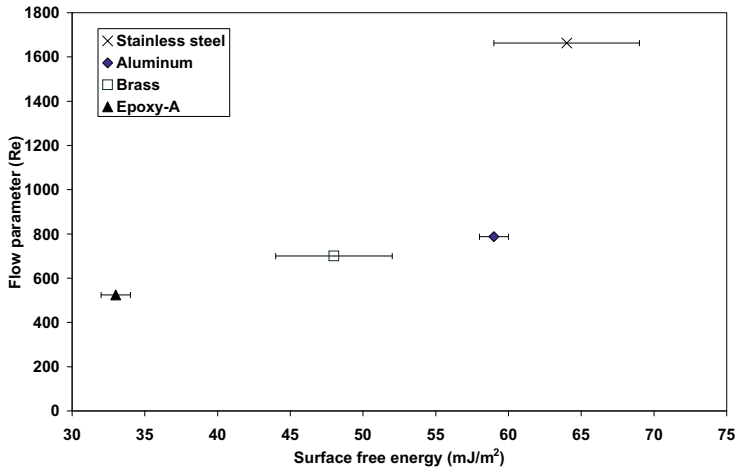
Figure 6.12: A plot of the dimensionless flow parameter (Reynolds number, Re) as a function of surface free energy of the metal surfaces. Figure adapted from Paper V, Figure 6.

any of the surfaces even at stirring rates up to 2000 rpm (Re $\approx$ 1700). The same was found when acids were added to the oil phase; the hydrate particles will not be detached. This may indicate that hydrates deposited on a pipeline surface will stay there, independent of the flow characteristics. However, it should be kept in mind that the droplet size and particle size will clearly influence the flow rate required to detach water/hydrate particles from the wall.

6.5   Summary of main results

Different solids have been investigated to determine whether the pipeline material has an influence on the deposition of hydrates to the pipeline wall during petroleum production. The influence of oil composition has also been investigated. The tasks were investigated by the means of contact angle

73

measurements and adhesion force measurements with a modified microme-chanical force apparatus.

It was shown that the adhesion force is dependent on the pipeline material and that the materials with lowest surface free energy have the lowest adhesion force between water and solid in oil, and between hydrate and a solid surface. The material investigated in this work with the lowest adhesion force was epoxy coated surfaces. However, it is important to note that the epoxy coated surface should be coated as smoothly as possible or the effect of using epoxy in preference to some of the other metals may be lost.

It was also found that acids reduce the adhesion force between water and solid in oil. The plugging index of different crude oils correlates relatively well with the measured adhesion force between stainless steel and water in crude oil, such that the least plugging oils leads to the lowest adhesion forces.

The presence of free water influences whether hydrates will deposit onto the pipeline wall. However, if a water drop deposit onto the pipeline surface, the flow needed to detach the water will be dependent on the pipeline material (e.g., surface free energy and roughness). Deposited hydrate particles will most likely not be detached and may begin growing from the pipe wall.

Chapter 7

Concluding remarks and further work

7.1 Conclusions

The influence of pipeline material and oil composition on the deposition of hydrates to the pipeline wall during petroleum production was investigated. The investigations were executed by the means of contact angle measurements and adhesion force measurements with a modified micromechanical force apparatus, in addition to considering the influence of flow.

Several factors have been identified as an influence on the deposition of hydrates to pipeline wall materials. These factors are listed here according to their assumed importance:

- Presence of free water; i.e., deposition will not occur unless free water is present.

- Pipeline material; i.e., deposition will be lowest on pipeline surface materials that have low surface free energy (e.g. epoxy coated surfaces).

It is also indicated that smooth surfaces leads to the lowest net adhesion forces.

- Crude oil composition; i.e., crude oils that are identified as non-plugging will also reduce deposition of hydrates to the pipeline wall. Petroleum acids are components that may reduce deposition.

Flow regimes will also influence deposition of hydrates and detachments after deposition. A hydrate particle that is deposited onto a water-wet pipeline wall will most likely remain deposited and not be detached independent of the pipeline flow. If water droplets deposit they may be detached, however it depends on the pipeline material properties as mentioned above.

7.2 Suggestions for further work

Further work investigating the effect of flow on the deposition of water/hydrates to the pipeline wall should be performed. This work has been initiated by Master student Maren A. Dahl at the University of Bergen. It was previously confirmed with a condensate flow loop that hydrates will deposit onto the pipeline wall [4]. Flow loop tests with epoxy coated pipelines and with varying amounts of acids in the oil phase could also give valuable knowledge.

The specific surface active components present in crude oils creating oil-wet pipeline surfaces and oil-wet hydrate surfaces should be identified. Zach Aman at the Colorado School of Mines has started investigating the effect of specific acid molecules contained in the naphthenic acids to identify the most active group of molecules.

Further, from field experience, hydrate plugs are often located in connection with pipeline bends, valves and risers. Hence, the impact of the pipeline geometry on water accumulation, heat transfer and flow pattern should be

considered. Positions in pipeline systems that are prone to plugging could be coated with a low surface free energy material, such as epoxy.

Development of a reproducible method for contact angle measurements on hydrate surfaces, which was initiated with Freon hydrates by Asserson [143], should be sought. This may simplify the search for surface active components that has affinity towards hydrate surfaces, and enhance the understanding of hydrates and wetting.

Bibliography

[1] E.D. Sloan. *Clathrate hydrates of natural gases.* Marcel Dekker, Inc., New York, Second edition, 1998.

[2] E.D. Sloan. A changing hydrate paradigm - from apprehension to avoidance to risk management. *Fluid Phase Equilibria*, 228-229:67–74, 2005.

[3] J.W. Nicholas, R.R. Inman, J.P.H. Steele, C.A. Koh, and Sloan E.D. A model approach to hydrate wall growth and sloughing in a water saturated gas pipeline. *Proceedings of the 6th International Conference on Gas Hydrates*, 2008.

[4] J.W. Nicholas, L.E. Dieker, L. Nuebling, B. Horn, H. He, C.A. Koh, and Sloan E.D. Experimental investigation of deposition and wall growth in water saturated hydrocarbon pipelines in the absence of free water. *Proceedings of the 6th International Conference on Gas Hydrates*, 2008.

[5] P.V. Hemmingsen, X. Li, and K. Kinnari. Hydrate plugging potential in underinhibited systems. *Proceedings of the 6th International Conference on Gas Hydrates*, 2008.

[6] D. Turner and L. Talley. Hydrate inhibition via cold flow - no chemical or insulation. *Proceedings of the 6th International Conference on Gas Hydrates*, 2008.

[7] F.H. Fadnes. Natural hydrate inhibiting components in crude oils. *Fluid Phase Equilibria*, 117:186–192, 1996.

[8] S. Høiland, K.M. Askvik, P. Fotland, E. Alagic, T. Barth, and F. Fadnes. Wettability of Freon hydrates in crude oil/brine emulsions. *Journal of Colloid and Interface Science*, 287:217–225, 2005.

[9] P.V. Hemmingsen, S. Kim, H.E. Pettersen, R.P. Rodgers, J. Sjöblom, and A.G. Marshall. Structural characterization and interfacial behavior

of acidic compounds extracted from north sea oil. *Energy & Fuels*, 20:1980–1987, 2006.

[10] P.V. Hemmingsen, X. Li, J.L. Peytavi, and J. Sjöblom. Hydrate plugging potential of original and modified crude oils. *Journal of dispersion science and technology*, 28:371–382, 2007.

[11] A.E. Borgund, K. Erstad, and T. Barth. Fractionation of crude oil acids by hplc and characterization of their properties and effects on gas hydrate surfaces. *Energy & Fuels*, 21:2816–2826, 2007.

[12] K. Erstad, S. Høiland, T. Barth, and P. Fotland. Isolation and molecular identification of hydrate surface active components in petroleum acid fractions. *Proceedings of the 6th International Conference on Gas Hydrates*, 2008.

[13] E.D. Sloan and C.A. Koh. *Clathrate hydrates of natural gases.* CRC Press, Third edition, 2008.

[14] webpage: http://chem.ps.uci.edu/∼kcjanda/Group/ Research−hydrates.html. 01-11-2009.

[15] E. G. Hammerschmidt. Formation of gas hydrates in natural gas transmission lines. *Industrial and Engineering Chemistry*, 26:851–855, 1934.

[16] J.G. Speight. *The Chemistry and Technology of Petroleum.* Marcel Dekker, Inc., New York, Third edition, 1999.

[17] E.D. Sloan. Clathrate hydrates: The other common solid water phase. *Industrial and Engineering Chemistry Research*, 39:3123–3129, 2000.

[18] M.A. Kelland. History of the development of Low Dosage Hydrate Inhibitors. *Energy and Fuels*, 20:825–847, 2006.

[19] C. Gaillard, J.P. Monfort, and J.L. Peytavy. Investigation of methane hydrate formation in a recirculating flow loop: Modeling of the kinetics and tests of efficiency of chemical additives on hydrate inhibition. *Oil and Gas Science and Technology - Reveue De L Institut Francais Du Petrole*, 54:365–374, 1999.

[20] L. Bergflødt. *Influence of crude oil based surface active components and synthetic surfactants on gas hydrate behaviour.* Department of Chemistry, University of Bergen, Norway, 2001. Dr.Scient. Thesis.

[21] M. Darbouret, M. Cournil, and J.M. Herri. Rheology study of tbab hydrate slurries as secondary two-ohase refrigerants. *International Journal of Refrigeration*, 28:663–671, 2005.

[22] S.H. Standal. *Wettabilitty of Solid Surfaces Induced by Adsorption of Polar Organic Components in Crude Oil.* Department of Chemistry, University of Bergen, Norway, 1999. Dr.Scient. Thesis.

[23] T. Young. *Miscellaneous Works.* Murray, London, 1855.

[24] W.G. Anderson. Wettability literature survey - part 1: Rock/oil/brine interactions and the effect of core handling on wettability. *Journal of Petroleum Technology*, 38:1125–1144, 1986.

[25] G. Cuicec. *Interfacial Phenomena in Petroleum recovery*, page 319. Dekker, New York, 1991.

[26] A.W. Neumann and R.J. Good. *Surface and Colloid Science.* Plenum, New York, 1979.

[27] D.N. Rao. Measurements of dynamic contact angles in solid-liquid-liquid systems at elevated pressures and temperatures. *Colloids and Surfaces A: Physicochemical and Engineering Aspects*, 206:203–216, 2002.

[28] D.N. Rao and R.S. Karyampudi. Application of the dual-drop dual-crystal contact angle technique to characterize heavy oil reservoir wettability. *Journal of Adhesion Science and Technology*, 16:581–598, 2002.

[29] G. Hansen, A.A. Hamouda, and R. Denoyel. The effect of pressure on contact angles and wettability in the mica/water/n-decane system and the calcite+stearic acid/water/n-decane system. *Colloids and Surfaces A: Physicochemical and Engineering Aspects*, 172:7–16, 2000.

[30] X. Xie, N.R. Morrow, and J.S. Buckley. Contact angle hysterisis and the stability of wetting changes induced by adsorption from crude oil. *Journal of Petroleum Science and Engineering*, 33:147–159, 2002.

[31] X. Xie and N.R. Morrow. Contact angles on quartz induced by adsorption of heteropolar hydrocarbons. *Journal of Adhesion Science and Technology*, 13:1119–1135, 1999.

[32] L. Chiappa, A. Menella, T.P. Lockhart, and G. Burrafato. Polymer adsorption at the brine/rock interface: the role of electrostatic interactions and wettability. *Journal of Petroleum Science and Engineering*, 24:113–122, 1999.

[33] K. Spildo and J.S. Buckley. Uniform and mixed wetting in square capillaries. *Journal of Petroleum Science and Engineering*, 24:145–154, 1999.

[34] D.Y. Kwok, C.J. Budziak, and A.W. Neumann. Measurements of static and low rate dynamic contact angles by means of an automated capillary rise technique. *Journal of Colloid and Interface Science*, 173:143–150, 1995.

[35] C. Atae-Allah, M. Cabrerizo-Vilchez, J.F. Gomez-Lopera, M. Holgado-Terriza, R. Roman-Roldan, and P.L. Luque-Escamilla. Measurement of surface tension and contact angle using entropic edge detection. *Measurement Science and Technology*, 12:288–298, 2001.

[36] O.I. del Rio and A.W. Neumann. Axisymmetric drop shape analysis: computational methods for the measurements of interfacial properties form the shape and dimensions of pendant and sessile drops. *Journal of Colloid and Interface Science*, 196:136–147, 1997.

[37] Y. Rotenberg, L. Boruvka, and A.W. Neumann. Determination of surface tension and contact angle form shape of the axisymmetric fluid interfaces. *Journal of Colloid and Interface Science*, 93:169–183, 1983.

[38] F.K. Skinner, Y. Rotenberg, and A.W. Neumann. Contact angle measurements from the contact diameter of sessile drops by means of a modified axisymmetric drop shape analysis. *Journal of Colloid and Interface Science*, 130:25–34, 1989.

[39] S.-Y. Yang, G.J. Hirasaki, S. Basu, and R. Vaidya. Mechanisms for contact angle hysterisis and advancing contact angles. *Journal of Petroleum Science Engineering*, 24:63–73, 1999.

[40] L. Liu and J.S. Buckley. Alteration of wetting of mica surfaces. *Journal of Petroleum Science and Engineering*, 24:75–83, 1999.

[41] S.H Al-Maamari and J.S. Buckley. Asphaltene precipitation and alteration of wetting: The potential for wettability changes during oil production. *SPE Reservoir Engineering & Evaluation*, 4:210–214, 2003.

[42] Y. Liu and J.S. Buckley. Evolution of wetting alteration by adsorption from crude oil. *SPE Formation and Evaluation*, 1:5–11, 1997.

[43] N.R. Morrow, G.Q. Tang, M. Valat, and X. and Xie. Prospects of improved oil recovery related to wettability and brine composition. *Journal of Petroleum Science Engineering*, 20:267–276, 1998.

[44] L. Skalli, J.S. Buckley, Y. Zhang, and N.R. Morrow. Surface and core wetting effects of surfactants in oil-based drilling fluids. *Journal of Petroleum Science Engineering*, 52:253–260, 2006.

[45] S. Standal, J. Haavik, A.M. Blokhus, and A. Skauge. Effect of polar organic components on wettability as studied by adsorption abd contact angles. *Journal of Petroleum Science and Engineering*, 24:131–144, 1999.

[46] S. Hoeiland, T. Barth, A.M. Blokhus, and A. Skauge. The effect of crude oil acid fractions on wettability as studied by interfacial tension and contact angels. *Journal of Petroleum Science and Engineering*, 30:91–103, 2001.

[47] C. Drummond and J. Israelachvili. Surface forces and wettability. *Journal of Petroleum Science and Engineering*, 33:123–133, 2002.

[48] M. Li, J. Su, Z. Wu, Y. Yang, and S. Ji. Study of the mechanisms of wax prevention in a pipeline with glass inner layer. *Colloids and Surfaces A: Physicochemical and Engineering Aspects*, 123-124:635–649, 1997.

[49] E.M. Freer, T. Svitova, and C.J. Radke. The role of interfacial rheology in reservoir mixed wettability. *Journal of Petroleum Science and Engineering*, 39:137–158, 2003.

[50] C.S. Vijapurapu and D.N. Rao. Compositional effects of fluids on spreading, adhesion and wettability in porous media. *Colloids and Surfaces A: Physicochemical and Engineering Aspects*, 241:335–342, 2004.

[51] K. Kumar, E. Dao, and K.K. Mohanty. Afm study of mineral wettability with reservoir oils. *Journal of Colloid and Interface Science*, 289:206–217, 2005.

[52] R.G. dos Santos, R.S. Mohamed, A.C. Bannwart, and W. Loh. Contact angle measurements and wetting behavior of inner surfaces of pipelines exposed to heavy crude oil and water. *Journal of Petroleum Science Engineering*, 51:9–16, 2006.

[53] K.M. Askvik, S. Høiland, P. Fotland, T. Barth, T. Grønn, and J. Fadnes. Calculation of wetting angles in crude oil/water/quartz systems. *Journal of Colloid and Interface Science*, 287:657–663, 2005.

[54] J.N. Israelachvili. *Intermolecular and surface forces.* Academic Press, London, 1991.

[55] Q. Zhao, Y. Liu, and E.W. Abel. Effect of temperature on the surface free energy of amorphous carbon films. *Journal of Colloid and Interface Science*, 280:174–183, 2004.

[56] E. Lugscheider and K. Bobzin. The influence on surface free energy of pvd-coatings. *Surface and Coatings Technology*, 142-144:755–760, 2001.

[57] E. Lugscheider, K. Bobzin, and M. Möller. The effect of pvd layer constitution on surface free energy. *Thin Solid Films*, 355-356:367–373, 1999.

[58] X. Zhang, J. Tian, L. Wang, and Z. Zhou. Wettability effects of coatings on drag reduction and paraffin deposition prevention in oil. *Journal of Petroleum Science and Engineering*, 36:87–95, 2002.

[59] P.K. Sharma and K.H. Rao. Analysis of different approaches for evaluation of surface energy of microbial cells by contact angle goniometry. *Advances in Colloid and Interface Science*, 98:341–463, 2002.

[60] D.Y. Kwok, H. Ng, and A.W. Neumann. Experimental study on contact angle patterns: liquid surface tensions less than solid surface tensions. *Journal of Colloid and Interface Science*, 225:323–328, 2000.

[61] F.M. Fowkes. Determination of interfacial tensions, contact angles, dispersion forces in surfaces by assuming additivity of intermolecular interactions in surfaces. *Journal of Physical Chemistry*, 66:382, 1962.

[62] F.M. Fowkes and M.A. Mostafa. Acid-base interactions in polymer adsorption. *Induatrial & Engineering Chemistry Product Research and Development*, 17:3–7, 1978.

[63] D.K. Owens and R.C. Wendt. Estimation of the surface free energy of polymers. *Journal of Applied Polymer Science*, 13:1741–1747, 1969.

[64] S. Wu and K.J. Brzozowski. Surface free energy and polarity of organic pigments. *Journal of Colloid Interface Science*, 37:686–690, 1971.

[65] C.J. van Oss, R.J. Good, and M.K. Chaudhury. The role of van der waals forces and hydrogen bonds in "hydrophobic interactions" between biopolymers and low energy surfaces. *Journal of Colloid and Interfacial Science*, 111:378–390, 1986.

[66] A.W. Neumann, R.J. Good, C.J. Hope, and Sejpal. An equation-of-state approach to determine surface tensions of low-energy solids from contact angles. *Journal of Colloid and Interface Science*, 49:291–304, 1974.

[67] D. Li and A.W. Neumann. A reformulation of the equation of state for interfacial tensions. *Journal of Colloid and Interface Science*, 137:304–307, 1990.

[68] D. Li and A.W. Neumann. Contact angles on hydrophobic solid surfaces and their interpretation. *Journal of Colloid and Interface Science*, 148:190–200, 1992.

[69] D.Y. Kwok and A.W. Neumann. Contact angle measurements and contact angle interpretation. *Advances in Colloid and Interface Science*, 81:167–249, 1999.

[70] D.Y. Kwok and A.W. Neumann. Contact angle interpretation in terms of solid surface tension. *Colloids and Surfaces A: Physicochemical and Engineering Aspects*, 161:31–48, 2000.

[71] H. Tavana, C.N.C. Lam, K. Grundke, P. Friedel, D.Y. Kwok, M.L. Hair, and A.W. Neumann. Contact angle measurements with liquids consisting of bulky molecules. *Journal of Colloid and Interface Science*, 279:493–502, 2004.

[72] H. Tavana, F. Simon, K. Grundke, D.Y. Kwok, M.L. Hair, and A.W. Neumann. Interpretation of contact angle measurements on two different fluoropolymers for the determination of solid surface tension. *Journal of Colloid and Interface Science*, 291:497–506, 2005.

[73] H. Tavana and A.W. Neumann. Recent progress in the determination of solid surface tensions from contact angles. *Advances in Colloid and Interface Science*, 132:1–32, 2007.

[74] D. Khang, S.Y. Kim, P. Liu-Snyder, G.T.R. Palmore, S.M. Durbin, and T.J. Webster. Enhanced fironectin adsorption on carbon nanotube/poly(carbonate) urethane: Independent role of surface nanoroughness and associated surface energy. *Biomaterials*, 28:4756–4768, 2007.

[75] D. Khang, J. Lu, C. Yao, K.M. Haberstroh, and T.J. Webster. The role of nanometer and sub-micron surface features on vascular and bone cell adhesion on titanium. *Biomaterials*, 29:970–983, 2008.

[76] W. Zhou, X. Zhong, X. Wu, L. Yuan, Z. Zhao, H. Wang, Y. Xia, Y. Feng, J. He, and W. Chen. The effect of surface roughness and wettability of nanostructured tio2 film on tca-8113 epithelial cells. *Surface Coating Technology*, 200:6155–6160, 2006.

[77] Q. Zhao, Y. Liu, C. Wang, S. Wang, N. Peng, and C. Jeynes. Reduction of bacterial adhesion on ion-implanted stainless steel surfaces. *Medical Engineering Physics*, 30:341–349, 2008.

[78] A. Thapa, T.J. Webster, and K.M. Haberstroh. Polymer with nano-dimensional surface features enhance bladder smooth cell adhesion. *Journal of Biomedical Materials Research*, 67A:1374–1383, 2003.

[79] S.M. Mirabedini, S. Pazoki, M. Esfandeh, M. Mohseni, and Z. Akbari. Comparison of drag characteristics of self-polishing co-polymers and silicone foul release coatings: A study of wettability and surface roughness. *Progress in Organic Coatings*, 57:421–429, 2006.

[80] J.R. Svendsen, G.M. Kontogeorgis, S. Kiil, C.E. Weinell, and M. Grønlund. Adhesion between coating layers based on epoxy and silicone. *Journal of Colloid and Interface Science*, 316:678–686, 2007.

[81] C.-M. Tåg, M. Juuti, K.-E. Peiponen, and J.B. Rosenholm. Print mottling: Solid-liquid adhesion related to optical appearance. *Colloids and Surfaces A: Physicochemical and Engineering Aspects*, 317:658–665, 2008.

[82] J. Katainen, M. Paajanen, E. Ahtola, V. Pore, and J. Lahtinen. Adhesion as an interplay between particle size and surface roughness. *Journal of Colloid and Interface Science*, 304:524–529, 2006.

[83] G. Huber, S.N. Gorb, N. Hosoda, R. Spolenak, and E. Artz. Influence of surface roughness on gecko adhesion. *Acta Biomaterials*, 3:607–610, 2007.

[84] K. Al-Anezi, D.J. Johnson, and N. Hildal. An atomic force microscope study of calcium carbonate adhesion to desalination process equipment: effect of anti-scale agent. *Desalination*, 59:359–370, 2008.

[85] H. Chen, M. Ishida, and T. Nakahara. Analysis of adhesion under wet conditions for three-dimensional contact considering surface roughness. *Wear*, 258:1209–1216, 2005.

[86] C.J. Taylor. *Adhesion force between hydrate particles and macroscopic investigation of hydrate film growth at the hydrocarbon/water interface.* Hydrate Research Center, Colorado School of Mines, Golden, USA, 2006. Master Thesis.

[87] R.M. Jorda. Paraffin deposition and prevention in oil wells. *Journal of Petroleum Technology*, 18:1605–1612, 1966.

[88] M.G. Donoso, A. Mèmdez-Vilas, J.M. Bruque, and M.L. Gonzàlez-Martin. On the relationship between common amplitude surface roughness parameters and surface area: Implications for the study of cell-material interactions. *International Biodeterioration & Biodegradation*, 59:245–251, 2007.

[89] C.D. Volpe, A. Penati, R. Peruzzi, S. Sibone, L. Toniolo, and C. Colombo. The combined effect of roughness and heterogeneity on contact angles: the case of polymer coating for stone protection. *Journal of Adhesion Science and Technology*, 14:273–299, 2000.

[90] C.D. Volpe, D. Maniglio, M. Morra, and S. Sibone. The determination of a 'stable-equilibrium' contact angle on heterogeneous and rough surfaces. *Colloids and Surfaces A: Physicochemical and Engineering Aspects*, 206:47–67, 2002.

[91] P.G. de Gennes, F. Brochard-Wyart, and D. Quéré. *Capillarity and Wetting Phenomena - Drops, Bubbles, Pearls, Waves.* Springer, New York, 2004.

[92] A.W. Neumann and J. Spelt. *Applied Surface Thermodynamics*, pages 109–168. Marcel Dekker, 1996.

[93] R.E. Johnson and R.H. Dettre. Contact angle, wettability and adhesion. *Advances in Chemistry Series*, 43:112–135, 1964.

[94] R.H. Dettre and R.E. Johnson. Contact angle, wettability and adhesion. *Advances in Chemistry Series*, 43:136–144, 1964.

[95] H.J. Busscher, A.W.J. van Pelt, H.P. de Boer, H.P. de Jong, and J. Arends. The effect of surface roughening of polymers on measured contact angles of liquids. *Colloids and Surfaces*, 9:319–331, 1984.

[96] G. Wolansky and Marmur A. Apparent contact angles on rough surfaces: the wenzel equation revisited. *Colloids and Surfaces A: Physicochemical and Engineering Aspects*, 156:381–388, 1999.

[97] D. Myers. *Surfaces, Interfaces and Colloids: Principles and Applications*. VCH, Weinheim, 1991.

[98] H. Kamusewitz, W. Possart, and D. Paul. The relation between young's equilibrium contact angle and the hysteresis on rough paraffin wax surfaces. *Colloids and surfaces A: Physicochemical and Engineering Aspects*, 156:271–279, 1999.

[99] P. Marcus. Surface science approach of corrosion phenomena. *Electrochimica Acta*, 43:109–118, 1998.

[100] S.H. Chen and C.W. Frank. Infrared and fluorescence spectroscopic studies of self-assembled n-alkanoic acid monolayers. *Langmuir*, 5:978–987, 1989.

[101] J. van der Brand, O. Blajiev, P.C.J. Beentjes, H. Terryn, and J.H.W. de Wit. Interaction of anhydride and carboxylic acid compounds with aluminum oxide surfaces studied using infrared reflection absorption spectroscopy. *Langmuir*, 20:6308–6317, 2004.

[102] A. Yurt, G. Bereket, and C. Ogretir. Quantum chemical studies on inhibition effect of amino acids and hydroxy carboxylic acids on pitting corrosion of aluminum alloy 7075 in nacl solution. *Journal of Molecular Structure: THEOCHEM*, 725:215–221, 2005.

[103] R.M. Wallace, P.J. Chen, S.A. Henck, and D.A. Webb. Adsoprtion of perfluorinated n-alkanoic acids on native aluminum oxide surfaces. *Journal of Vacuum Science and Technology A*, 13:1345–1350, 1995.

[104] P.J. Chen, R.M. Wallace, and S.A. Henck. Thermal properties of perfluorinated n-alkanoic acids self-assembled on native aluminum oxide surfaces. *Journal of Vacuum Science and Technology A*, 16:700–706, 1998.

[105] D.L. Allara and R.G. Nuzzo. Spontaneously organized molecular assemblies. 1. formation, dynamics, and physical properties of n-alkanoic acids adsorbed from solution on an oxidized aluminum surface. *Langmuir*, 1:45–52, 1985.

[106] D.L. Allara and R.G. Nuzzo. Spontaneously organized molecular assemblies. 2. quantitative infrared spectroscopic determination of equilibrium structures of solution-adsorbed n-alkanoic acids on an oxidized aluminum surface. *Langmuir*, 1:52–66, 1985.

[107] L.H. Dubois, B.R. Zegarski, and R.G. Nuzzo. Spontaneous organization of carboxylic acid monolayer film in ultrahigh vakuum. kinetics conctraint to assembly via gas-phase adsorption. *Langmuir*, 2:412–417, 1986.

[108] A.H.M. Sondag and F.J. Touwslager. Order-disorder transition as a function of surface coverage for 1-hexadecanoic acid chemisorbed on oxidized aluminum. lateral interaction effects on the carboxylate band and macroscopic manifestation of the transition. *Langmuir*, 10:1023–1027, 1994.

[109] J. van der Brand, O. Blajiev, P.C.J. Beentjes, H. Terryn, and J.H.W. de Wit. Interaction of ester functional groups with aluminum oxide surfaces studied using infrared reflection absorption spectroscopy. *Langmuir*, 20:6318–6326, 2004.

[110] A.W. Adamson. *Physical chemistry of Surfaces.* John Wiley & Sons, New York, fifth edition, 1990.

[111] G.A. Parks. The isoelectric points of solid oxides, solid hydroxides, and aqueous hydroxo complex systems. *Chemical Reviews*, 65:177–198, 1965.

[112] E. McCafferty and J.P. Wightman. Determination of the surface isoelectric point of oxide films on metals by contact angle titration. *Journal of Colloid and Interface Science*, 194:344–355, 1997.

[113] D. Chvedov and E.L.B. Logan. Surface cahrge properties of oxides and hydroxides formed on metal substrates determined by contact angle tittration. *Colloids and Surfaces A: Physicochemical and Engineering Aspects*, 240:211–223, 2004.

[114] M. Kosmulski. ph-dependent surface chargeing and point of zero charge iii. update. *Journal of Colloid and Interface Scince*, 298:730–741, 2006.

[115] N. Kallevik, D. Kovacevic, I. Dedic, and Tomasic. Effect of corrosion on the isoelectric point of stainless steel. *Corrosion*, 50:598–602, 1994.

[116] C.S. Wang and J.Y. Shieh. Synthesis and properties of epoxy resins containing bis(3-hydroxyphenyl) phenyl phosphate. *European Polymer Journal*, 36:443–452, 2000.

[117] S.A. Kumar, T. Balakrishnan, M. Alagar, and Z. Denchev. Development and characterization of silicone/phosphorus modified epoxy materials and their application as anticorrosion and antifouling coatings. *Progress in Organic Coatings*, 55:207–217, 2006.

[118] X.-H. Yang, W.-L. Zhu, Z. Lin, and J.-J. Huo. Aerodynamic evaluation of an internal epoxy coating in nature gas pipeline. *Progress in Organic Coatings*, 54:73–77, 2005.

[119] webpage: http://pslc.ws/mactest/eposyn.htm. 01-11-2009.

[120] D. Waples. *Geochemistry in geochemical exploration*. Reidel Publishing Company, Holland, 1985.

[121] W. Meredith, S.-J. Kelland, and D.M. Jones. Influence of biodegradation on crude oil activity and carboxylic acid composition. *Organic Geochemistry*, 31:1059–1073, 2000.

[122] K.E. Peters and J.M. Moldowan. *The Biomarker Guide*, pages 252–265. Prentice-Hall, New Jersey, 1993.

[123] L.M. Wenger, C.L. David, and G.H Isaksen. Multiple controls on petroleum biodegradation and impact on oil quality. *Society of Petroleum Engineer paper 71450*, 2001.

[124] J. Connan. *Advances in petroleum geochemistry*, chapter Biodegradation of crude oils in reservoirs, pages 299–335. Academic Press, London, 1984.

[125] T. Barth, S. Høiland, P. Fotland, K.M. Askvik, B.S. Pedersen, and A.E. Borgund. Acidic compounds in biodegraded petroleum. *Organic Chemistry*, 35:1513–1525, 2004.

[126] M.S. Arney, G.S. Ribeiro, E. Guevara, R. Bai, and D.D. Joseph. Cement-lined pipes for water lubricated transport of heavy oil. *International Journal of Multiphase Flow*, 22:207–221, 1996.

[127] J.S. Buckley. Effective wettability of minerals exposed to crude oil. *Current Opinion in Colloid & Interface Science*, 6:191–196, 2001.

90

[128] M.S. Akhlaq, P. Götze, D. Kessel, and W. Dornow. Adsorption of crude oil colloids on glass plates: measurements of contact angles and the factors influencing glass surface properties. *Colloids and Surfaces A: Physicochemical and Engineering Aspects*, 126:25–32, 1997.

[129] A. Graue, E. Aspenes, T. Bognø, and R.W. Moe. Alteration of wettability and wettability heterogeneity. *Journal of Petroleum Science and Engineering*, 33:3–17, 2002.

[130] M.H. Sayyouh, A.M. Hemeida, M.S. Al-Blehed, and S.M. Desouky. Role of polar compounds in crude oils on rock wettability. *Journal of Petroleum Science and Engineering*, 6:225–233, 1991.

[131] G. González and Moreira M.B.C. The wettability of mineral surfaces containing adsorbed asphaltene. *Colloids and Surfaces*, 58:293–302, 1991.

[132] M.O. Denekas, C.C. Mattax, and G.T. Davis. Effect of crude oil components on rock wettability. *Transactions of the American Institute of Mining and Metallurgical Engineers*, 216:330–333, 1959.

[133] J.S. Buckley and D.L. Lord. Wettability and morphology of mica surfaces after exposure to crude oil. *Journal of Petroleum Science and Engineering*, 39:261–273, 2003.

[134] R. Hamadou, M. Khodja, M. Kartout, and A. Jada. Permeability reduction by asphaltene and resins deposition in porous media. *Fuel*, 87:2178–2185, 2008.

[135] J.S. Buckley, Y. Liu, X. Xie, and N.R. Morrow. Asphaltene and crude oil wetting - the effect of oil composition. *SPE Journal*, 2:107–119, 1997.

[136] S.-Y. Yang, G.J. Hirasaki, S. Basu, and R. Vaidya. Statistical analysis on parameters that effecy wetting for crude oil/brine/mica systems. *Journal of Petroleum Science Engineering*, 33:203–215, 2002.

[137] J.S. Buckley. Wetting alteration of solid surfaces by crude oils and their asphaltenes. *Revue de l'Institut Français du Pétrole*, 53:303–312, 1998.

[138] J.S. Buckley, Y. Liu, and Monstersleet. Mechanisms of wetting alteration by crude oils. *SPE Journal*, 54:54–61, 1998.

[139] C. Drummond and J. Israelachvili. Fundamental studies of crude oil-surface water interactions and its relationship to reservoir wettability. *Journal of Petroleum Science and Engineering*, 45:61–81, 2004.

[140] E.M. Bryant, R.S. Bowman, and J.S. Buckley. Wetting alteration of mica surfaces with polyethoxylated amine surfactants. *Journal of Petroleum Science and Engineering*, 52:244–252, 2006.

[141] J.S. Buckley and Y. Liu. Some machanisms of crude oil/brine/solid interactions. *Journal of Petroleum Science and Engineering*, 20:155–160, 1998.

[142] S. Høiland, A.E. Borgund, T. Barth, P. Fotland, and K.M. Askvik. Wettability of Freon hydrates in crude oil/brine emulsions: the effect of chemical additives. *Proceedings of the 5th International Conference on Gas Hydrates*, 4:1151–1161, 2005.

[143] R.B. Asserson. *Interfacial tension measurements of Freon hydrates by means of droplet deposition and contact angle measurements.* Department of Physics and Technology, University of Bergen, Norway, 2007. Master thesis.

[144] L.E. Dieker, Aman Z.M., N.C. George, A.K. Sum, E.D. Sloan, and C.A. Koh. Micromechanical adhesion force measurements between hydrate particles in hydrocarbon oils and theri modifications. *Accepted for publication in Energy & Fuels*, 2009.

[145] P. Finkle, H.D. Draper, and J.H. Hildebrand. The theory of emulsification. *Journal of the American Chemical Society*, 45:2780–2788, 1923.

[146] B.P. Binks. Particles as surfactants - similarities and differences. *Current Opinion in Colloid and Interfacial Science*, 7:21–41, 2002.

[147] R. Aveyard, B.P. Binks, and J.H. Clint. Emulsion stabilised solely by colloidal particles. *Advances in Colloid and Interface Science*, 100-102:503–546, 2003.

[148] A.E. Borgund, S. Høiland, T. Barth, P. Fotland, R.A. Kini, and R. Larsen. *Proceedings of the 6th International Conference on Gas Hydrates*, 2008.

[149] W.K. Seifert and W.G. Howells. Interfacially active acids in a California crude oil. *Analytical Chemistry*, 41:554–562, 1969.

[150] G.C. Laredo, C.R. López, R.E. Álvarez, and J.L. Cano. Naphthenic acids, total acid number and sulfur content profile characterization in Isthmus and Maya crude oil. *Fuel*, 83:1689–1695, 2004.

[151] W.K. Seifert. Effect of phenols on the interfacially activity of crude oil (California) carboxylic acids and the identification of carbazoles and indoles. *Analytical Chemistry*, 41:562–568, 1969.

[152] E. Babaian-Kibala. Phosphate ester inhibitors solve naphthenic acid corrosion problems. *Oil and Gas Journal*, 92(9):31–35, 1994.

[153] X.Q. Wu, H.M. Jing, Y.G. Zheng, Z.M. Yao, and W. Ke. Resistance of Mo-bearing stainless steels and Mo-bearing stainless-steel coating to naphthenic acid corrosion and erosion-corrosion. *Corrosion Science*, 46:1013–1032, 2004.

[154] B.P. Tissot and D.H. Welte. *Petroleum Formation and Occurrence*. Springer Verlag, Berlin Heidelberg, Second Revised and Enlarged edition, 1984.

[155] J.S. Clemente, M.D. MacKinnon, and P.M. Fedorak. Aerobic biodegradation of two commercial naphthenic acids preparations. *Environmental Science and Technology*, 38:1009–1016, 2004.

[156] J.S. Clemente and P.M. Fedorak. A review of the occurence, analysis, toxicity, and the biodegradation of naphthenic acids. *Chemosphere*, 60:585–600, 2005.

[157] S. Acevedo, G. Escobar, M.A. Ranaudo, J. Khazen, B. Borges, J.C. Pereira, and B. Méndez. Isolation and characterization of low and high molecular weight acidic compounds from Cerro Negro extraheavy crude oil. Role of these acids in the interfacial properties of the crude oil emulsions. *Energy & Fuels*, 13:333–335, 1999.

[158] R. Gunde, A. Kumar, S. Lehnart-Batar, R. Mäder, and E.J. Windhab. Measurement of the surface and interfacial tension from maximum volume of a pendant drop. *Journal of Colloid and Interface Science*, 244:113–122, 2001.

[159] N. Aske, H. Kallevik, and J. Sjöblom. Water-in-crude oil emulsion stability by critical electric field measurements. correlation to physico-chemical parameters and near-infrared spectroscopy. *Journal of Petroleum Science and Engineering*, 36:1–17, 2002.

[160] J. Sjöblom, N. Aske, I.H. Auflem, Ø. Brandal, T.E. Havre, Ø. Sæther, A. Westvik, E.E. Johnsen, and H. Kallevik. Our current understanding of water-in-crude oil emulsions. Recent characterization techniques and high pressure performance. *Advances in Colloid and Interfacial Science*, 100-102:399–473, 2003.

[161] W.F. McClure. Near-infrared spectroscopy. the giant is running strong. *Analytical Chemistry*, 66:43A–53A, 1994.

[162] H. Kallevik, O.M. Kvalheim, and J. Sjöblom. Quantitative determination of asphaltenes and resins in solution by means of near-infrared spectroscopy. correlations to emulsion stability. *Journal of Colloid and Interface Science*, 225:494–504, 2000.

[163] H. Aakre, T. Solbakken, and R.B. Scüller. An in-line nir/endoscope technique for observations in real hydrocarbon multiphase systems. *Flow Measurements and Instrumentation*, 16:289–293, 2005.

[164] J. Tomas. Adhesion of ultrafine particles - a micromechanical approach. *Chemical Engineering Science*, 62:1997–2010, 2007.

[165] V.A. Parsegian. *Van der Waals forces, A handbook for biologists, chemists, engineers and physicists.* Cambridge University Press, New York, 2006.

[166] Z. Adamczyk. Particle adsorption and deposition: role of electrostatic interactions. *Advances in Colloid and Interface Science*, 100-102:267–347, 2003.

[167] Z. Adamczyk and P. Weroński. Role of electrostatic interactions in particle adsorption. *Advances in Colloid and Interface Science*, 63:41–149, 1996.

[168] Z. Adamczyk and P. Weroński. Application of the dlvo theory for particle depostion problems. *Advances in Colloid and Interface Science*, 83:137–226, 1999.

[169] Z. Adamczyk, Siwek B., Zembala M., and Belouschek P. Kinetics of localized adsorption of colloid particles. *Advances in Colloid and Interface Science*, 48:151–280, 1994.

[170] C. Yang, T. Dabros, D. Li, H. Czarnecki, and J.H. Masliyah. Kinetics of particle transport to a solid surface from an impinging jet under surface and external force fields. *Journal of Colloid and Interface Science*, 208:226–240, 1998.

[171] R. Chein and W. Liao. Analysis of particle-wall interactions during particle free fall. *Journal of Colloid and Interface Science*, 288:104–113, 2005.

[172] S. Kim and C.J. Lawrence. Suspension mechanics for particle contamination control. *Chemical Engineering Science*, 43:991–1016, 1988.

[173] B.D. Bowen, S. Levine, and Epstein N. Fine particle deposition in laminar flow trough parallel-plate and cylindrical channels. *Journal of Colloid and Interface Science*, 54:375–390, 1976.

[174] H. Krupp. Particle adhesion theory and experiment. *Advances in colloid and interface science*, 1:111–239, 1967.

[175] M. Götzinger and Peukert W. Particle adhesion force distribution on rough surfaces. *Langmuir*, 20:5298–5303, 2004.

[176] B.V. Derjaguin and L.D. Landau. Theory of the stability of strongly charged lyophobic sols and the adhesion of strongly charged particles in solutions of elctrolytes. *Acta Physicochimica, URSS*, 14:633–662, 1941.

[177] E.J.W. Vervey and J.T.G. Overbeek. *Theory of the stability of lyophobic colloids*. Elsevier, Amsterdam, New York, 1948.

[178] O.H. Pakarinen, A.S. Foster, M. Paajanen, T. Kalinainen, J. Katainen, I. Makkonen, J. Lahtinen, and R.M. Nieminen. Towards an accurate description of the capillary force in nanoparticle-surface interactions. *Modelling and Simulation in Materials Science and Engineering*, 13:1175–1186, 2005.

[179] J. Jang, Schartz G.C., and M.A. Ratner. Capillary force in atomic force microscopy. *Journal of Chemical Physics*, 120:1157–1160, 2004.

[180] R. Camargo and T. Palermo. Rheological properties of hydrate suspensions in an asphaltenic crude oil. *Proceedings of the 4th International Conference on Gas Hydrates*, 2002.

[181] S.-O. Yang, D.M. Kleehammer, Z. Huo, E.D. Sloan, and K.T. Miller. Temperature dependence of particle-particle adherence force in ice and clathrate hydrates. *Journal of Colloid and Interface Science*, 277:335–341, 2004.

[182] C.J. Taylor, L.E. Dieker, K.T. Miller, C.A. Koh, and E.D. SSloan Jr. Micromechanical adhesion force measurements between ttetrahydrofuran hydrate particles. *Journal of Colloid and Interface Science*, 306:255–261, 2007.

[183] L.E. Dieker, C.J. Taylor, C.A. Koh, and E.D. Sloan. Micromechanical adhesion force measurements between cyclopentane hydrate particles. *Proceedings of the 6th International Conference on Gas Hydrates*, 2008.

[184] J.W. Nicholas, L.E. Dieker, E.D. Sloan, and C.A. Koh. Assessing the feasibility of hydrate deposition on pipeline wall - adhesion force measurements of clathrate hydrate particles on carbon steel. *Journal of Colloid and Interface Science*, 331:322–328, 2009.

[185] T. Austvik. *Hydrate Formation and Behaviour in Pipes. Division of Thermodynamics*. Norwegian University of Science and Technology, Trondheim, Norway, 1992. PhD thesis.

[186] J.S. Gudmundsen. *Proceedings of the 4th International Conference on Gas Hydrates, Yokohama, Japan*, page 912, 2002.

[187] A. Lund, D. Lysne, R. Larsen, and K. Hjarbo. *Norwegian Patent, No. 311854*, 2002.

[188] A. Lund, R. Larsen, and K.W. Hjarbo. Methods and system for transporting a flow of fluid hydrocarbons containing water. *US Pub. No. US 2004/0176650 A1*, 2004.

[189] M. Wolden, A. Lund, N. Oza, T. Makogon, C.B. Argo, and R. Larsen. Cold flow black oil slurry transport of suspended hydrate and wax solids. *Proceedings of the 5th International Conference on Gas Hydrates*, 2005.

[190] R. Larsen, A. Lund, C. Argo, and T. Makogon. Cold flow - a simple multiphase transport solution for harsh environments. *Proceedings of 18th International Oil Field Chemsitry Symposium, Geilo, Norway*, 2007.

[191] L.D. Talley, D.J. Turner, and D.K. Priedeman. Method for generating a non-plugging hydrate slurry. *Patent WO 2007/095399*, 2007.

[192] T. Sugimoto, T. Takahashi, H. Itoh, S.-I. Sato, and A. Muramatsu. Direct measurement of interparticle forces by the optical trapping technique. *Langmuir*, 13:5528–5530, 1997.

96

[193] A.K. Yeung and R.P. Pelton. Micromechanics: a new approach to study the strength and breakup of flocs. *Journal of Colloid and Interface Science*, 184:579–585, 1996.

[194] S.J.R. Simons and R.J. Fairbrother. Direct observations of liquid binder-particle interactions: the role of wetting behavior agglomerate growth. *Powder Technology*, 110:44–58, 2000.

[195] W.R. Bowen, R.W. Lovitt, and Wright C.J. Application of atomic force microscopy to the study of micromechanical properties of biological materials. *Biotechnology Letters*, 22:893–903, 2000.

[196] A. Döppenschmidt, M. Kappl, and H.J. Butt. Surface properties of ice studied by atomic force microscopy. *Journal of Physical Chemistry B*, 110:7813–7819, 1998.

[197] X. Fan, P. Ten, C. Clarke, A. Bramley, and Zhang Z. Direct adhesion of the adhesive force between ice particles by micromanipulation. *Powder Technology*, 131:105–110, 2003.

[198] L.E. Dieker. *Cyclopentane hydrate interparticle adhesion force measurements*. Hydrate Research Center, Colorado School of Mines, Golden, USA, 2009. Master Thesis.

[199] J.W. Nicholas. *Hydrate deposition in water saturated liquid condensate pipeline*. Hydrate Research Center, Colorado School of Mines, Golden, USA, 2008. PhD Thesis.

[200] C.W. Macaosko. *Rheology Principles, Measurements and Applications*. Wiley-VCH, New York, 1994.

[201] P. Kosinski and A.C. Hoffmann. Extension of the hard-sphere particle-wall collision model to account for particel deposition. *Physical review E*, 79(6):XXX, 2009.

[202] H. Pedersen. *Formation, particle size distribution and flow dependence of Freon (R11) hydrates in multiphase flow systems*. Department of Physics and Technology, University of Bergen, Norway, 2008. Master Thesis.

[203] Z. Kilinc. *Formation and particle size distribution of cyclopentane hydrates in a multiphase flow system*. Department of Physics and Technology, University of Bergen, Norway, 2008. Master Thesis.

[204] W.L. McCabe, J.C. Smith, and P. Harriott. *Unit Operations of Chemical Engineering*. McGraw - Hill, 2005.

[205] W. Shen, J. Kim, and C.J. Kim. Controlling the adhesion force for electrostatic actuation of microscale mercury drop by physical surface modifications. *Proceedings from IEEE international conference on micro electro mechanical systems, Las Vegas*, pages 52–55, 2002.

[206] A. Theodorakakos, T. Ous, M. Gavaises, J.M. Nouri, N. Nikolopoulos, and H. Yanagihara. Dynamics of water droplets detached from porous surfaces of relevance to pem fuel cells. *Journal of Colloid and Interface Science*, 300:673–687, 2006.

[207] P.C Hiemenz and R. Rajagopalan. *Principles of Colloid and Surface Chemistry*, pages 339–340. Taylor & Francis Group, 1997.

[208] M.N. Lingelem, A.I. Majeed, and E. Stange. Industrial experience in evaluation of hydrate formation, inhibition and dissociation in pipeline design and operation. *Proceedings of International Conference on Natural Gas Hydrates*, 715:75–93, 1994.

[209] T. Austvik, E. Hustvedt, B. Meland, L.I. Berge, and D. Lysne. Tommeliten gamma field hydrate experiments. *Proceedings of 7th BHRA International Conference on Multiphase Flow*, 1995.

[210] A.S. Guariguata. *Jamming mechanisms of hydrate particles: Experiments and modeling*. Hydrate Research Center, Colorado School of Mines, Golden, USA, 2009. Master Thesis.

[211] B. Podgornik, B. Zajec, S. Strnad, and K. Stana-Kleinschek. Influence of surface energy on the interactions between coatings and lubricants. *Wear*, 262:1199–1204, 2007.